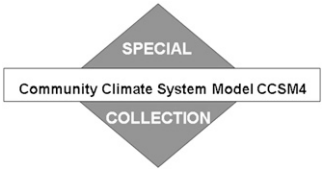

Mean and Variability of the Tropical Atlantic Ocean in the CCSM4*

ERNESTO MUÑOZ

New Mexico Consortium, Los Alamos, New Mexico, and National Center for Atmospheric Research, Boulder, Colorado

WILBERT WEIJER

Los Alamos National Laboratory, and New Mexico Consortium, Los Alamos, New Mexico

SEMYON A. GRODSKY

University of Maryland, College Park, College Park, Maryland

SUSAN C. BATES

National Center for Atmospheric Research, Boulder, Colorado

ILANA WAINER

University of Sao Paulo, Sao Paulo, Brazil

(Manuscript received 19 May 2011, in final form 17 February 2012)

ABSTRACT

This study analyzes important aspects of the tropical Atlantic Ocean from simulations of the fourth version of the Community Climate System Model (CCSM4): the mean sea surface temperature (SST) and wind stress, the Atlantic warm pools, the principal modes of SST variability, and the heat budget in the Benguela region. The main goal was to assess the similarities and differences between the CCSM4 simulations and observations. The results indicate that the tropical Atlantic overall is realistic in CCSM4. However, there are still significant biases in the CCSM4 Atlantic SSTs, with a colder tropical North Atlantic and a hotter tropical South Atlantic, that are related to biases in the wind stress. These are also reflected in the Atlantic warm pools in April and September, with its volume greater than in observations in April and smaller than in observations in September. The variability of SSTs in the tropical Atlantic is well represented in CCSM4. However, in the equatorial and tropical South Atlantic regions, CCSM4 has two distinct modes of variability, in contrast to observed behavior. A model heat budget analysis of the Benguela region indicates that the variability of the upper-ocean temperature is dominated by vertical advection, followed by meridional advection.

1. Introduction

It is important to understand the climate dynamics in the tropical Atlantic basin. The tropical Atlantic impacts the climate of Northeast Brazil, northwestern Africa, Central America, and the Caribbean regions. The tropical Atlantic is also important because of its remote impacts on the tropical Pacific (Ding et al. 2012; Losada et al. 2010; Saravanan and Chang 2000) and on the Indian Ocean (Kucharski et al. 2007, 2008, 2009). Even though the tropical Atlantic has been recognized as an important region in the earth's coupled climate system, it has been challenging to model adequately by coupled climate models. A few recent reports summarize the advances in the understanding of the tropical Atlantic climate and its variability (e.g., Hurrell et al. 2006; Xie and Carton 2004; Garzoli and Servain 2003; Visbeck

* Supplemental information related to this paper is available at the Journals Online website: http://dx.doi.org/10.1175/JCLI-D-11-00294.s1.

Corresponding author address: Ernesto Muñoz, National Center for Atmospheric Research, NESL/CGD/OS, P.O. Box 3000, Boulder, CO 80307-3000.
E-mail: emunoz@ucar.edu

DOI: 10.1175/JCLI-D-11-00294.1

et al. 2001). Some of the main aspects of the tropical Atlantic Ocean discussed in the current study include the seasonal cycles and interannual variability of wind stress, sea surface temperature (SST), the Atlantic warm pool (WP), and a head budget of the Benguela region.

The seasonal cycle of SST in the tropical Atlantic is related to the seasonal cycles of wind stress and of the intertropical convergence zone (ITCZ). The seasonal cycle is the largest ocean–atmosphere signal in the region. As discussed in Servain et al. (1998), the timing and characteristics of the seasonal evolution of SST, winds, and the ITCZ depend on the coupled air–sea–land dynamics (Schouten et al. 2005). For example, when the precipitation is greatest over the equatorial Amazon in boreal spring, the equatorial easterlies are weak and Atlantic SSTs are quasi-uniform in the near-equatorial belt. As the seasons progress, the ITCZ shifts northward and stronger southeasterly winds amplify the eastward tilt of the thermocline, leading (through upwelling and Kelvin waves) to a colder eastern equatorial Atlantic in late spring and early summer. Farther north in the Caribbean Sea, the low-level (~925 hPa) zonal winds have a semiannual cycle with peaks in February and July (Muñoz et al. 2008), given the seasonal changes in pressure and thermal wind. The Caribbean low-level jet affects precipitation in the Caribbean and Central America, and it also affects regional SST (Small et al. 2007; Muñoz et al. 2008; Wang et al. 2008) through coastal upwelling.

A significant aspect of the tropical Atlantic seasonal cycle is its warm pool. Warm pools have been defined as those regions of the ocean with temperatures greater than 28.5°C (Tian et al. 2001; Wang and Enfield 2003). Beyond its surface manifestation and extent, the WP in the tropical Atlantic has vertical and horizontal profiles that are important with respect to the heat content of the upper layer of the ocean. The Atlantic WP has a component in the northwestern tropical Atlantic spanning the Gulf of Mexico and the Caribbean Sea [i.e., the Intra-Americas Sea (IAS)] that peaks during boreal summer and early fall (Lee et al. 2007; Enfield and Lee 2005; Wang and Enfield 2003). The heat content in the tropical North Atlantic (TNA) WP is an important regulator of the air–sea interactions in tropical storms and hurricanes passing through that region (Wang et al. 2006; Landsea et al. 1999; Gray 1990). The impact of the TNA-WP SSTs extends to the tropical Pacific through an upper-level Gill-type circulation (Saravanan and Chang 2000; Wang et al. 2008). In contrast to the TNA-WP, much less attention has been given to the tropical South Atlantic (TSA) warm pool, where SSTs also exceed 28.5°C during boreal spring.

A majority of coupled general circulation models (GCMs) have biases in the mean state of both the tropical Pacific and Atlantic, including notorious warm biases in the southeastern tropical basins (Davey et al. 2002; Large and Danabasoglu 2006; Zuidema et al. 2011). In the tropical Atlantic, the most severe warm SST bias (in excess of 5°C) occurs along the Benguela coast of southwestern Africa (e.g., Chang et al. 2007; Richter and Xie 2008), that is, the TSA warm pool region. This spurious pool of abnormally warm water simulated by most coupled climate models alters the large-scale meridional SST gradient across the tropical Atlantic and thus may project onto the natural mode of the tropical Atlantic variability, known as the meridional or interhemispheric SST mode (e.g., Xie and Carton 2004). Furthermore, some coupled models also have relaxed (weaker) easterly winds along the equator related to weaker precipitation over the Amazon region that is in turn related to the warm bias in the eastern equatorial Atlantic (Doi et al. 2012; Tozuka et al. 2011; Richter et al. 2012; Wahl et al. 2011; Richter and Xie 2008; Chang et al. 2007). Chang et al. (2007) and Richter and Xie (2008) have shown that abnormally weak equatorial easterly wind is responsible in part for the time-mean warm bias of the Benguela SST. Tozuka et al. (2011) showed that the magnitude of the SST bias is related to differences in the convection parameterization in atmospheric models.

In addition to remote mechanisms, the impact of local meridional winds and upwelling on the Benguela SST has been discussed by Large and Danabasoglu (2006). They show that the warm bias in eastern boundary upwelling regions in the Community Climate System Model (CCSM) is due to a combination of weak ocean currents, weak upwelling, weak alongshore wind, too little stratus cloud, and neighboring mountainous regions. The impact of local upwelling is emphasized by Grodsky et al. (2012), who argue that adequate representation of the magnitude of the southerly Benguela low-level wind jet (Nicholson 2010) is crucial for maintaining the zonal sea level gradient in the coastal ocean and thus cold water transport by the coastal jet of the Benguela Current. Independent of its origin, any warm SST bias in the Benguela region may grow and expand via the positive feedbacks from marine stratocumulus clouds (e.g., Ma et al. 1996; Philander et al. 1996; Medeiros 2011).

Observed changes in Atlantic SST occur on a wide range of time scales (Keenlyside and Latif 2007; Dommenget and Latif 2000). On multidecadal time scales, the Atlantic multidecadal oscillation (Enfield et al. 2001) is mostly confined to the North Atlantic and possibly reflects changes in the strength of the Atlantic meridional overturning circulation (AMOC; Danabasoglu et al. 2012b; Muñoz et al. 2011). At decadal time scales, the out-of-phase variations of SST in the northern and

southern tropical Atlantic (NTA and STA, respectively) are driven by the wind–evaporation–SST (WES) feedback in the trade winds (Carton et al. 1996; Chang et al. 1997). At interannual time scales, remote impacts of the El Niño–Southern Oscillation (ENSO; Enfield and Mayer 1997; Deser et al. 2006) and the North Atlantic Oscillation (Czaja et al. 2002) produce different SST responses in the northern and southern tropical sectors and thus contribute to the observed lack of coherence between SST variations in the two regions. Deser et al. (2006) found that in CCSM, version 3 (CCSM3), the correlation between the tropical Pacific Niño-3 SST index in December–February (DJF) and tropical North Atlantic SST anomalies in March–May (MAM) was similar to the correlation from observations. However, in CCSM3 the tropical Pacific Niño-3 index had a high correlation with SSTs in the deep tropical Atlantic (between 3°N and 10°S) that is not observed in the same analysis from observations (Deser et al. 2006).

In addition to a tropical Atlantic lagged response to ENSO, there is increasing evidence (based on observations and modeling studies) that the equatorial Atlantic SST anomalies are anticorrelated with tropical Pacific SSTs as an intrinsic phenomenon. This tropical Pacific–Atlantic interbasin anticorrelation is also evident (and more widespread) in the sea level pressure (SLP) anomalies. Some studies that make this evident are Hastenrath (1990), Giannini et al. (2000), Wang (2006), Muñoz et al. (2008), García-Serrano et al. (2008), Polo et al. (2008), Losada et al. (2010), and Ding et al. (2012). For example, it is observed from Fig. 8 in Polo et al. (2008) that the equatorial Atlantic SST anomalies lead the Pacific Niño-3 index with an anticorrelation greatest at 8 months. Also, it is observed from Fig. 14 in Muñoz et al. (2008) that the interbasin gradients of SST and SLP are highly correlated to the variations in the strength of the Caribbean low-level jet. Explanations of this interbasin gradient mode of variability has been provided by Wang (2006), García-Serrano et al. (2008), Polo et al. (2008), Losada et al. (2010), and Ding et al. (2012).

The variability of tropical Atlantic SSTs has been observed to have a few main modes that are predominant at different times of the year (Ruiz-Barradas et al. 2000; Hu et al. 2008; Hu and Huang 2007; Foltz and McPhaden 2010; Servain et al. 1990, 2003). One of the modes of variability is the so-called meridional mode or interhemispheric mode and is the dominant mode in the boreal spring (Servain et al. 1998; Mahajan et al. 2010). The meridional mode is characterized by a north–south gradient of SST anomalies from one subtropical region to its counterpart in the other hemisphere, and a pattern of surface wind anomalies from the colder subtropics to the warmer subtropics (Murtugudde et al. 2002; Nobre and Shukla 1996; Hastenrath and Heller 1977). Another mode of variability is the so-called zonal mode or Atlantic Niño and is predominant in the boreal summer (Servain 1991; Tokinaga and Xie 2011; Carton and Huang 1994; Zebiak 1993; Shannon et al. 1986). Yet, the identification of tropical Atlantic modes of SST variability has also benefited from the use of statistical techniques, such as rotated empirical orthogonal functions (rEOFs). The resulting modes using rEOFs have been referred to as the STA pattern, the NTA pattern, and the southern subtropical Atlantic (SSA) pattern (Huang and Shukla 2005; Bates 2008). Previous studies have analyzed these modes and the dynamics and thermodynamics that explain their variability (Bates 2008, 2010; Huang and Shukla 2005; Florenchie et al. 2004; Chang et al. 1997; Carton et al. 1996; Shannon et al. 1987). These periodic changes of SST in the northern and southern tropical Atlantic displace the ITCZ and affect rainfall over surrounding continents in northeastern Brazil and the African Sahel [see, e.g., Robertson et al. (2003); Xie and Carton (2004), and references therein].

Observation-based analyses of SST variability in the tropical Atlantic indicate that the standard deviation of anomalous SST is strongest in areas adjacent to the western coast of Africa (Doi et al. 2010), and that it reaches a maximum in the Angola–Benguela Frontal Zone [referred to as the Benguela region in this paper; see, e.g., Florenchie et al. (2003)]. SSTs in the Benguela region are affected by local and remote impacts according to observations and model simulations (Rouault et al. 2007, 2009; Hirst and Hastenrath 1983; Colberg and Reason 2007b; Lubbecke et al. 2010; Richter et al. 2010; Florenchie et al. 2003). Florenchie et al. (2003) have suggested a link between the Benguela warm events and weakening of the zonal equatorial winds 1–2 months in advance, which remotely impact the Benguela region via Kelvin waves propagating eastward along the equator and farther south along the coast. Richter et al. (2010) have demonstrated based on observations and model simulations that the impact of local upwelling on Benguela SST is comparable to the remote impact of the equatorial winds.

The recent availability of the CCSM, version 4 (CCSM4), provides an opportunity to reassess the status of the simulation of the tropical Atlantic by one of the leading coupled climate models. In this study the main aspects of the tropical Atlantic Ocean are analyzed, expanding on the CCSM3 analysis of the tropical Atlantic by Deser et al. (2006) and other CCSM3 studies. The model simulations, the observations, and the methodology used are described in section 2. We provide some standard diagnostics for CCSM4 comparison to the CCSM3 and

to observations, and evaluate how well the CCSM4 is able to simulate the tropical Atlantic seasonal cycle (in section 3), including the Atlantic warm pools. We then discuss how the CCSM4 compares to observations relative to the interannual variability of the Atlantic warm pools and SSTs (section 4), including a detailed analysis of the model upper-ocean heat budget in the Benguela region. A summary and a discussion are presented as the final section of the manuscript.

2. Data and methods

a. Model data

The main CCSM4 dataset analyzed is an ensemble of five twentieth-century (20C) CCSM4 simulations (these were archived as b40.20th.track1.1deg.[005–009] and are referred to here as runs R005–R009). These CCSM4 ensemble simulations were run in the same manner with the exception of their initial state. Each of the CCSM4 members was initialized from the 1850 control simulation, with the five initializations chosen to represent different states of the AMOC. The period used for the analyses in this study spans 1950–2005 of the CCSM4 20C simulations. Complete descriptions of these simulations are provided by Gent et al. (2011). The CCSM4 20C ensemble simulations were compared to observations, to a CCSM3 20C ensemble mean, and to an ocean–sea ice hindcast experiment forced by observed winds.

The ocean–sea ice hindcast simulation [Parallel Ocean Program–Coordinated Ocean-Ice Reference Experiments (''POP-CORE'')] was conducted using the CCSM4 ocean model POP (with a nominal 1° horizontal resolution) coupled to an active freely evolving dynamic–thermodynamic sea ice model [Los Alamos Sea Ice Model (CICE)]. Monthly climatological river runoff in the POP-CORE is based on Dai et al. (2004) discharge estimates. The model was forced by four cycles of the CORE version 2 interannual forcing data (Large and Yeager 2009), which span the 60-yr period from 1948 to 2007. The POP-CORE data analyzed are from the fourth (last) forcing cycle. No data assimilation is done in this POP-CORE simulation. The SSTs were not restored to observations. Although, as described in Griffies et al. (2009), bulk formulas are used to compute turbulent heat fluxes from a prescribed, time-evolving atmospheric state, which influences the SSTs.

There were eight ensemble members in the CCSM3 simulations, and when possible, all eight members are used. One of the ensemble members did not contain monthly output and therefore is not used in the annual cycle comparisons. The CCSM3 ensemble members were initialized from the 1870 control simulation (the control was switched to 1850 for CCSM4) at 20-yr intervals with no tie to a physical feature [see Table 1 of Gent et al. (2006) for details on CCSM3 simulations]. The CCSM3 simulations ended in December of 1999; therefore, the 20-yr mean used in this study is from 1980 to 1999.

Differences between CCSM3 and CCSM4 are expected due to various changes in the model physics and the spinup and tuning procedures, which are all intended to produce a more realistic model. Both sets of simulations are the nominal 1° resolution in all components; however, this resolution has increased in the atmospheric and land components from approximately 1.4° in CCSM3 to approximately 1° in CCSM4. There are 26 vertical levels in the atmospheric component [Community Atmosphere Model, version 4 (CAM4)] of CCSM4. The depth resolution of the ocean model has also increased from 40 levels in CCSM3 to 60 levels in CCSM4, with the majority of the additional layers in the upper ocean. The dynamical core is different in the atmospheric component (Neale et al. 2012, manuscript submitted to *J. Climate*): the ice model component, with a new radiation scheme and different albedo values, produces different sea ice cover (Holland et al. 2012); and the addition of new ocean parameterizations include more ocean physics than were present in CCSM3 (Danabasoglu et al. 2012a). Because of differences in model tuning and spinup (Gent et al. 2011), the ocean in the CCSM3 20C simulations loses heat over the length of the run, while in the CCSM4 simulations it more realistically gains heat.

A control CCSM4 run was also used to evaluate the variability of the heat budget in the Benguela region. The monthly averaged fields were from the 1° 1850 control run with 1300 yr of simulation forced by fixed preindustrial levels of ozone, solar, volcanic, greenhouse gases, carbon, and sulfur dioxide–trioxide (archived as b40.1850.track1.1deg.006). The Benguela heat budget analysis focuses on data from a 97-yr period (model years 863–959). A sensitivity examination has been carried out to ensure that the climatology of this particular period is similar to that of later periods.

b. Observational data

For the comparisons of the mean and seasonal cycle of SST and wind stress, the observations used include SST from Hurrell et al. (2008) and wind stress derived from the CORE (Griffies et al. 2009; Large and Yeager 2009) dataset. The periods used from these observations were 1980–99 when comparing with CCSM3 ensemble means and 1986–2005 when comparing with CCSM4 ensemble means. These datasets and periods are chosen since they are used in the literature to assess the CCSM and are

also used in publications within this special collection to assess ocean behavior.

For analyses of the Atlantic warm pools, two observational datasets with subsurface temperatures were used: the *World Ocean Atlas 2009* (*WOA09*; Locarnini et al. 2010; Levitus et al. 1998, hereafter L98) and the Ishii et al. (2003, hereafter I2003) temperature datasets. The L98 12-month climatology has been used in many other studies of the mean state of the ocean, including the Intra-Americas Sea warm pool study of Wang and Enfield (2003). The L98 climatology provides climatological temperature data for the 12 calendar months based on *available* observations during the period from the year 1773 to the year 2008 (as indicated in the metadata). Also used is the observational dataset developed by I2003 with monthly temperature data interpolated to a $1° \times 1°$ grid. For the warm pool estimates, the averages from the I2003 products were computed based on the period 1950–2005. Both of these observational datasets have the same horizontal $1° \times 1°$ grid and the same vertical levels, with data at the surface and at 10, 20, 30, 50, 75, 100, 125, 150, 200, 250, and 100-m intervals between 300 and 700 m.

The Extended Reconstructed SST version 3b (ERSSTv3b; Smith et al. 2008) observational dataset is used to compute rEOFs of SSTs.

c. Methods

For the warm pool analysis, since the vertical resolution of the model data is finer than that of the observational datasets, the model data were linearly interpolated to the vertical levels of the observations before calculating the depth of the 28.5°C isotherm (Z28.5) as a metric of the warm pool. Once Z28.5 was calculated, the result was interpolated to the horizontal grid of the observational products at each month. These monthly values of Atlantic warm pool volume were used to calculate the warm pool mean, seasonal cycle, and other statistics, such as rank histograms.

Rank histograms from the time series of the Atlantic WP were computed according to Hamill (2001). To create the rank histogram, the five CCSM4 ensemble simulations are considered in addition to an observational estimate [either I2003 or the POP-CORE simulation], thereby having six bins in the histogram. For each time step (month) in the WP time series, the ensemble member simulations are ranked from lowest to highest after including the estimate from observations. As explained by Hamill (2001), if there is equal probability that the observation will fall in each bin, then the histogram should be uniformly distributed or flat, and one can conclude that on the average, the ensemble spread represents correctly the uncertainty. However, if the histogram is distributed nonuniformly, one can refer either to underdispersion or to overdispersion of the ensemble (Hamill 2001).

To compare the main modes of tropical Atlantic SST variability, rEOF were computed from the CCSM4 20C simulations, the POP-CORE hindcast, and the ERSSTv3b observational product. The area of interest is the Atlantic Ocean between 30°S and 30°N, and the analysis is performed for the period 1948–2005, the era common to these datasets. In contrast to many previous studies, the Caribbean and Gulf of Mexico SSTs are included in these EOF analyses of the tropical Atlantic; including the region of the IAS accounts for the influence of teleconnections on the subtropical North Atlantic SSTs (Muñoz et al. 2010). First, an EOF analysis is performed on the area-weighted, linearly detrended, monthly anomaly time series of SST, to focus on internal variability and to reduce the impact of secular warming trends. The EOFs and their principal components (PCs) are renormalized so that the PCs have unit variance and the EOFs carry the standard deviation (von Storch 2002). Then a varimax rotation is applied to the dominant 10 EOFs (i.e., the 10 dominant spatial patterns). The rotation technique removes the orthogonality constraint on the EOFs and leads to more localized spatial patterns that might be easier to interpret in terms of dynamical processes (Richman 1986; Dommenget and Latif 2002).

A heat budget analysis of the upper-ocean layer in the Benguela region was performed to quantify relative contributions of the air–sea heat fluxes versus heat advection terms. To evaluate relative impacts of heat advection and the surface fluxes on anomalous heat content, we focus on the relationship between the terms of the vertically integrated heat balance Eq. (1) spatially averaged over the Benguela region. In common notations the vertically integrated heat balance equation is

$$C_p\rho\int_{z=-H}^{z=0}\frac{\partial T}{\partial t}dz = C_p\rho\int_{z=-H}^{z=0}\left(-u\frac{\partial T}{\partial x} - v\frac{\partial T}{\partial y} - w\frac{\partial T}{\partial z}\right)dz + \mathrm{NSHF} - \mathrm{VDIFF}(z=-H) + R,$$

where NSHF is the net surface heat flux and vertical integration is taken down to $H = 80$ m. In this region $H = 80$ m is below the mixed-layer year-round. We focus only on the terms available in the history files of CCSM4 output, and so the vertical diffusion VDIFF($z = H$) is combined in R with other unresolved terms that include lateral diffusion, diffusion introduced by the mixed layer model, and errors due to the use of monthly (instead of model) sampling to calculate the time derivative in (1). Heat advection terms on the right-hand

side of (1) are computed on the original model grid using the POP numerics.

3. Long-term mean and seasonal cycle

a. Time mean of wind stress and SST

In this section we perform standard diagnostics used to assess previous versions of the CCSM to quantify progress in the CCSM4. Figure 1 shows the mean state of zonal and meridional wind stress from observations, and the difference with CCSM3 and CCSM4. The overall pattern of easterlies throughout the tropics with centers near 15°S (southeasterlies) and 15°N (northeasterlies) is captured by both CCSM4 and CCSM3 (Fig. 1). The direction of the wind stress, for the most part, seems to be correct in the model. Yet, the magnitude of the wind stress is the main difference between the model and the observations, as observed in Figs. 1b,c.

As in the CCSM3, the CCSM4 exhibits wind stress smaller in magnitude than the CORE wind stress throughout the equatorial (deep tropics) region (Figs. 1b,c). In the western basin, this is mostly due to weakened easterlies, and in the eastern basin weakened southerlies are responsible for the decrease in magnitude (Bates et al. 2012). Both of these differences are related to a reduced upwelling in the east. From the model–observations differences in SST (Fig. 2), it is observed that there are warm SST biases along the equator and in the tropical southeastern Atlantic. Along the equator, observations indicate a west-to-east, warm-to-cold SST gradient. CCSM3 exhibited a zonal SST gradient opposite of that from observations. In contrast, the CCSM4 shows significant improvement in the SST gradient along the equator, with SSTs in the western basin closer to those from observations (Fig. 2c). However, the observed temperature zonal gradient is still not captured in CCSM4.

In the regions of strongest easterlies (centered around 15°N–S), the wind stress in CCSM4 is enhanced over CORE, with the largest differences in the eastern basin near the African continent and in the southern Caribbean region. In general, these differences have been reduced in CCSM4 compared to CCSM3 (Fig. 1); yet, they still contribute to biases in the SSTs (Fig. 2). For example, the largest SST differences within the 30°S–30°N domain are found in the southern Caribbean Sea and in the southeastern basin along the coast of Africa (Figs. 2a,b). Nonetheless, as with wind stress, these SST differences have improved in CCSM4. In the southern Caribbean Sea, the SST model–observations difference has improved from −4.0° (in CCSM3) to −2.5°C (in CCSM4). However, in the southeastern basin near the African coast, the SST difference has increased from 6.5° (in CCSM3) to 7.5°C (in CCSM4), approximately.

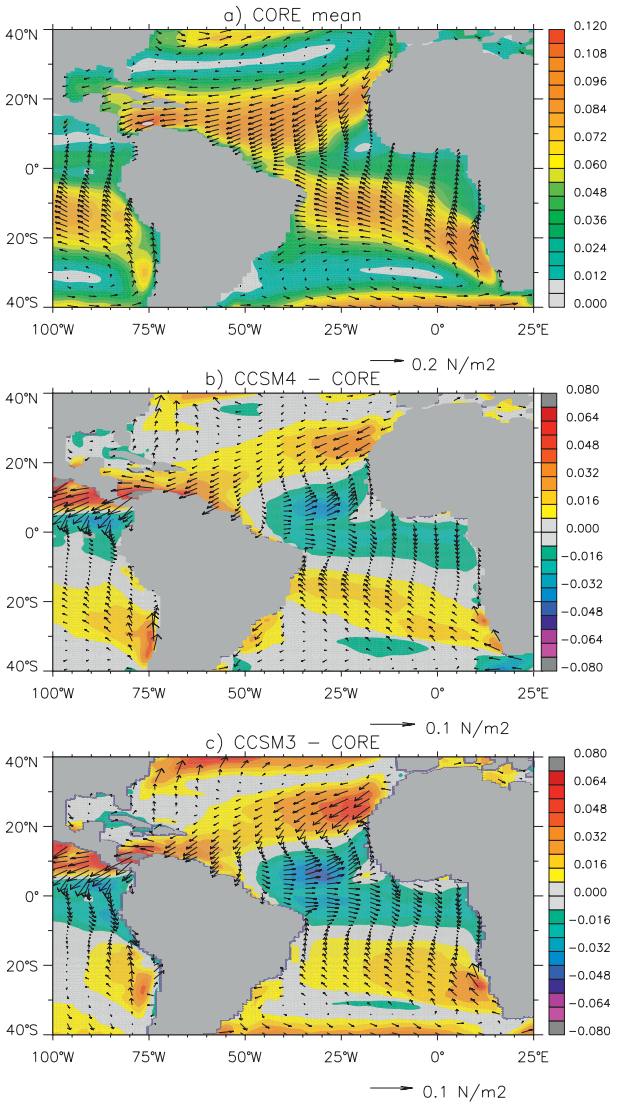

FIG. 1. (top) Total mean CORE-based wind stress derived for the period 1980–2005. Model- minus CORE-based difference for (middle) CCSM4 and (bottom) CCSM3. Period used for each model is explained in the text. Shading indicates wind stress magnitude, and vectors indicate the direction. Units are N m^{-2}.

In the tropical Atlantic (as in the global ocean), a shift to warmer surface ocean temperatures is noted in the CCSM4 versus CCSM3 (Danabasoglu et al. 2012a) (this shift is mostly due to the spinup procedure effects described in the data and methods section). The mean values from 30°S to 30°N of the tropical Atlantic SST difference from observations (excluding the Mediterranean Sea) are −0.50°C for CCSM3 and 0.41°C for CCSM4, reflecting the warming shift. The root-mean-square (RMS) error of the SST differences over the

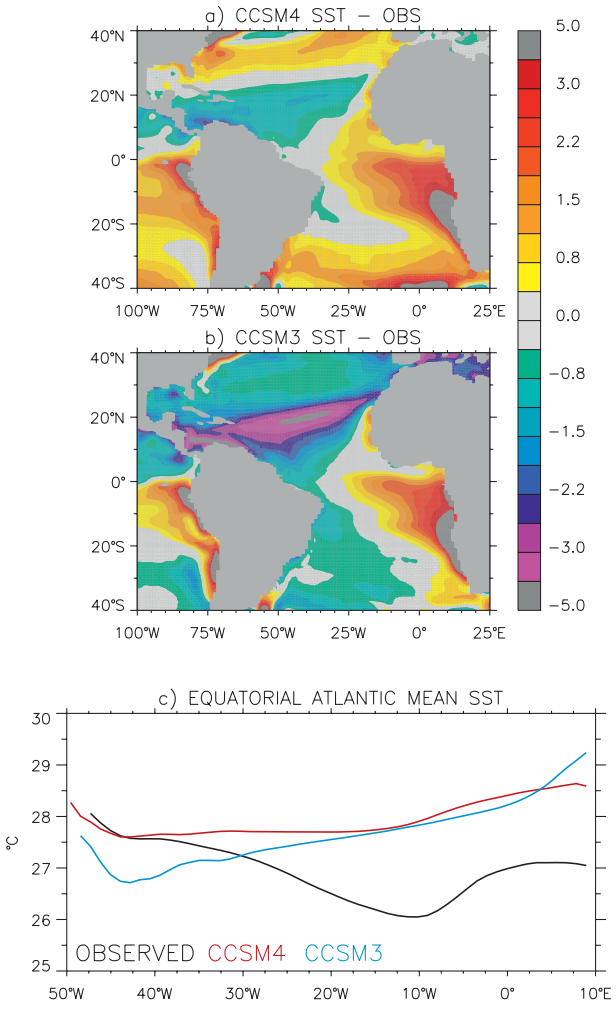

FIG. 2. Model minus observations of mean SST (°C) for (a) CCSM4 and (b) CCSM3; (these correspond to Fig. 6 from Danabasoglu et al. (2012a) with a focus on the tropical Atlantic. (c) Mean SST along the equator from observations (black line, 1980–2005), CCSM4 (red line, 1986–2005), and CCSM3 (blue line, 1980–99).

same region does show improvement, with a value of 1.65°C for CCSM3 and 1.20°C for CCSM4. Therefore, the improvements in TNA SSTs described above are influenced by both the overall warming in the transition from CCSM3 to CCSM4 and the improvements in the mean wind stress field.

b. *Seasonal cycle of wind stress and equatorial SST*

In Fig. 3, we present the seasonal cycle of wind stress from CORE observations (left panels) along with the difference from CCSM4 (right panels). In all seasons, wind stress in CCSM4 is too weak in the deep tropics and too strong at higher tropical latitudes. The largest and most widespread of these differences occurs during DJF and MAM, corresponding to the seasons when the equatorial easterlies are the weakest and monsoonal flow in the Gulf of Guinea is the strongest. The weakened easterlies are related to the incorrect SST gradient along the equator, and perhaps the model is underrepresenting the land–sea temperature difference driving the monsoonal flow. In MAM, a large difference in the southerly wind stress occurs in the central basin just north of the equator. This difference is due to the displacement of the largest cross-equatorial flow westward in CCSM4; in CORE this maximum occurs in the central basin.

In all of the areas described above, the mean bias of wind stress influences the seasonal bias quite strongly. Therefore, we also compare the wind stress seasonal departure from the annual mean (figures not shown). Compared to observations the amplitude of the zonal wind stress in the Caribbean Sea is weaker in June–August (JJA) and stronger in September–November (SON). In the TNA centered at 25°N and next to the African coast, where northeasterly winds dominate, we find the zonal wind stress difference to be the largest in DJF and also present in MAM, and the meridional wind stress weakened in DJF and strengthened in JJA. In the TSA we find the same pattern of southerlies (too weak in the Gulf of Guinea and too strong to the south) to be present in DJF, with opposite sign differences occurring in JJA (southerlies too strong in the Gulf of Guinea and too weak to the south).

Figure 4 shows the SST monthly departure from the annual mean, which helps in assessing the phasing and magnitude of the seasonal cycle. The seasonal cycle of SST along the equator in the CCSM4 has improved greatly over the CCSM3 (Fig. 4), most likely due to improvements in the wind stress forcing from the atmosphere. Most notable of these improvements is found in the warm phase in late boreal winter and spring. In CCSM3, the warm phase begins in the western basin and propagates eastward, neither of which occur in the observations and are corrected in the CCSM4. Though the phasing in the CCSM4 lags observations by approximately half a month, the character and magnitude are quite similar (Fig. 4).

c. *Seasonal cycle of the Atlantic warm pool*

Figures 5a–d show the month of the calendar year when the 28.5°C isotherm is deepest in the long-term mean. When the CCSM4 ensemble mean is compared to the L98 and the I2003 datasets, a better agreement in the WP is obtained between CCSM4 and I2003. For example, in both the CCSM4 and the I2003 datasets, the Z28.5 is present throughout the TSA; in the TNA the Z28.5 crosses the basin at about 10°N in both

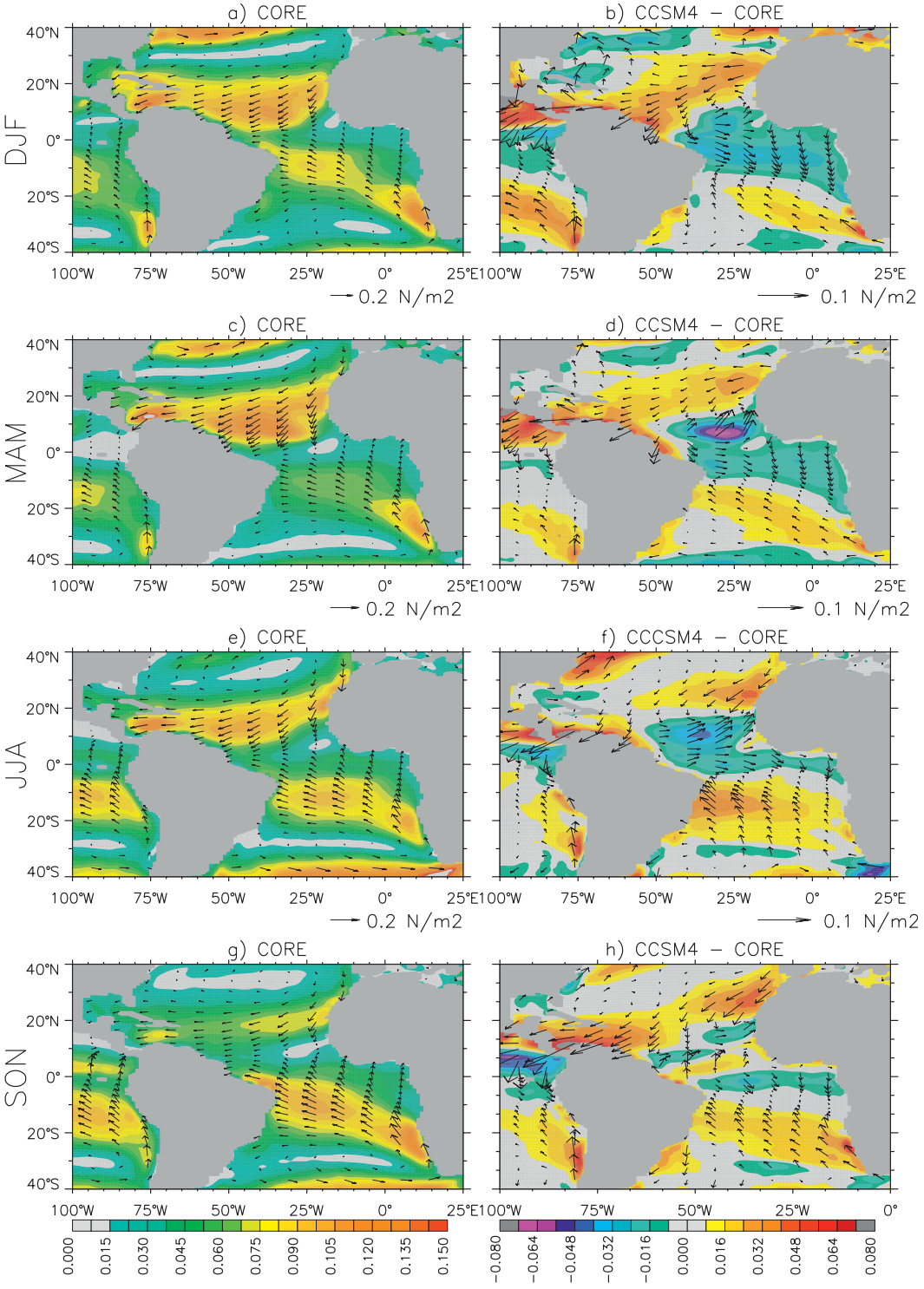

FIG. 3. (left) Seasonal means of the CORE-based wind stress. (right) Seasonal differences of the CCSM4 wind stress minus CORE-based wind stress. The units are N m^{-2}, and the period used for both CORE and CCSM4 is 1986–2005. Shading indicates magnitude, and the vectors are the direction.

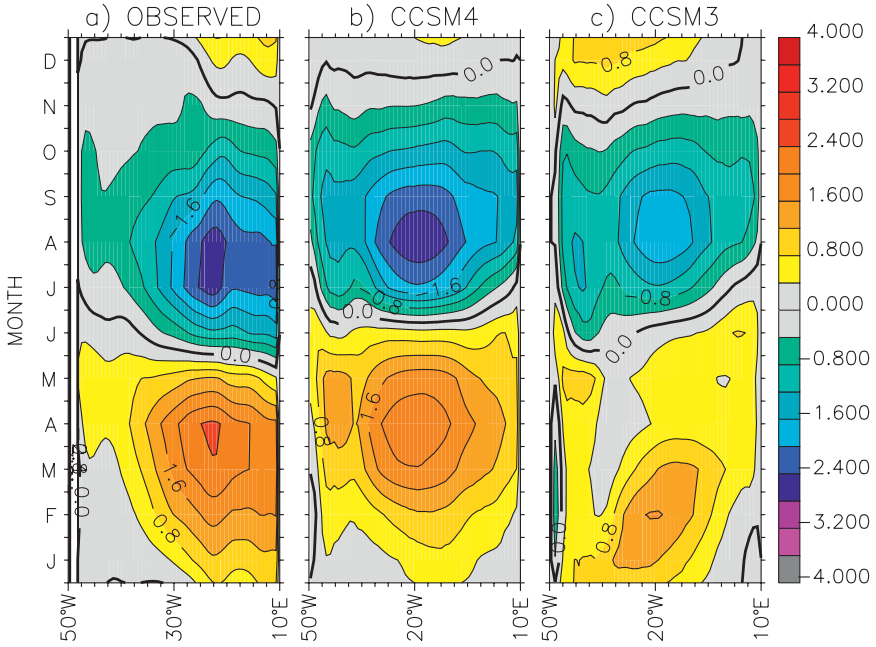

FIG. 4. Seasonal cycle of SST along the equator calculated as the mean of each month minus the total mean for (a) observations, (b) CCSM4, and (c) CCSM3. Units are °C, and the seasonal cycles are calculated over 1980–99 for CCSM3, 1986–2005 for CCSM4, and 1980–2005 for observations.

products. Yet, the warm pool extent and timing in the POP-CORE hindcast seems to match better the I2003 observational estimates, indicating that some of the major differences between CCSM4 and the observations are in the coupled framework (not strictly in the ocean component of CCSM4: POP).

The seasonal cycle of the warm pool volume in the tropical Atlantic is shown in Fig. 5e. In all products there are relative maxima in boreal spring and in boreal summer, indicating greater extent in April and in September, respectively. The peak in April corresponds to the TSA warm pool (TSA-WP), whereas the peak in September corresponds to TNA-WP (Figs. 5a–d). The TSA-WP in observations is smaller than its northern counterpart, the TNA-WP. The major differences in the TNA-WP and the TSA-WP between model and observations are described below.

In the TNA, the main differences in the CCSM4 and the POP-CORE hindcast are in the Caribbean Sea. Both the CCSM4 and the POP-CORE show a Z28.5 in the northern Caribbean Sea deepest in November. However, in the L98 and the I2003 observational products, the Caribbean Z28.5 is deepest in October. Figure 6 shows the mean warm pool in September, when the TNA warm pool has its greatest volume (Fig. 5e). Among the similarities in all products is the presence of a warm pool deepest between Cuba and Central America with Z28.5 greater than 60 m. The POP-CORE simulation and the I2003 observational estimates have September warm pools very similar in spatial extent, that is to say, extending to the southern Caribbean Sea, to the northeast of the Antilles, and across the basin approximately between 5° and 15°N. Yet, in CCSM4 as in L98, there is a lack of subsurface temperatures greater than 28.5C in the southern Caribbean Sea. In the CCSM4 this is related to the strong zonal wind stress along the southern Caribbean Sea (as observed in Fig. 3). This stronger Caribbean low-level jet would induce stronger upwelling in the southern Caribbean Sea, thereby simulating temperatures colder than observations and reducing the volume of the warm pool.

In the TSA, a main difference between the Z28.5 from observations and from CCSM4 is the timing of the deepest Z28.5 in the TSA (Fig. 5). In the Gulf of Guinea and Benguela regions, the observations have the deepest Z28.5 in March and April, respectively, while the CCSM4 has its deepest Z28.5 in May. This indicates that the CCSM4 is staying warmer than observations during the decay of the TSA warm pool in the eastern TSA. April is the month of greatest volume of Z28.5 in the TSA (Figs. 5, 7). Yet, as observed from the seasonal cycle in Fig. 5e, in the CCSM4 the WP volume in April exceeds that of September (whereas in observations the

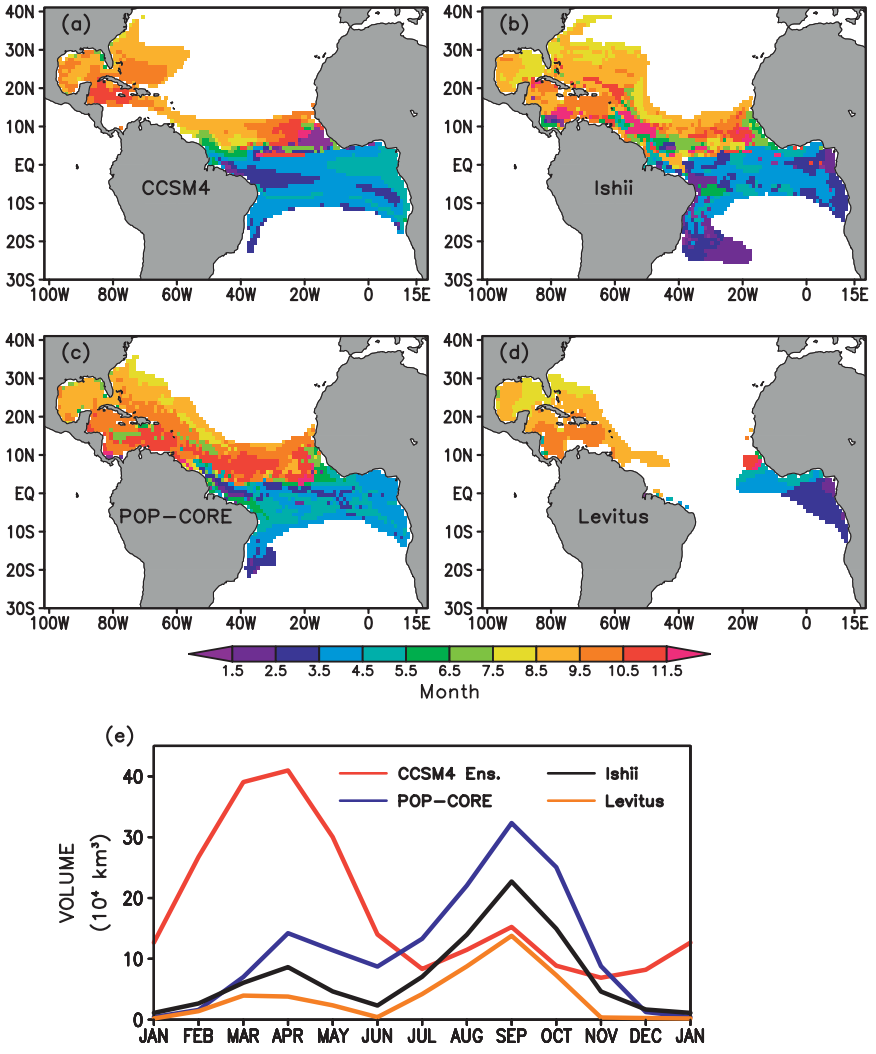

FIG. 5. (a)–(d) Horizontal distribution of the month of deepest 28.5°C isotherm from the long-term mean from 1950 to 2005. The numbers 1–12 correspond to the months from January to December. The Pacific data have been masked. (a) The CCSM4 ensemble mean and (c) the POP ocean model forced with CORE surface forcing. (b),(d) The observational products I2003 and Levitus (1998), respectively. (e) Seasonal cycle of the volume of the 28.5°C isotherm between 40°S and 40°N.

WP is largest in boreal summer–fall and peaking in September). This greater TSA warm pool during boreal spring seems to be associated with the pattern of wind stress biases in CCSM4 from December to March. As observed from Fig. 4, the wind stress magnitude in CCSM4 is weaker than in observations in an area collocated with the TSA warm pool in the boreal springtime (as in Fig. 7a). The weaker wind stress in the TSA reduces the evaporative cooling in the region. Furthermore, in the tropical southeastern Atlantic, the meridional wind stress in CCSM4 is weaker than in observations, thereby reducing the upwelling along the eastern boundary and reducing the intensity of the Benguela Current, the Angola Current, and the Atlantic south equatorial current systems, which normally advect cold water from the south.

4. Tropical Atlantic variability

a. Atlantic warm pools

The September time series of TNA volume (km^3) encompassed by the 28.5°C isotherm (i.e., the TNA-WP) are shown in Fig. 6e. The volume was calculated from the 5°N latitude to the north and across the basin. The I2003 observational products show anomalously large

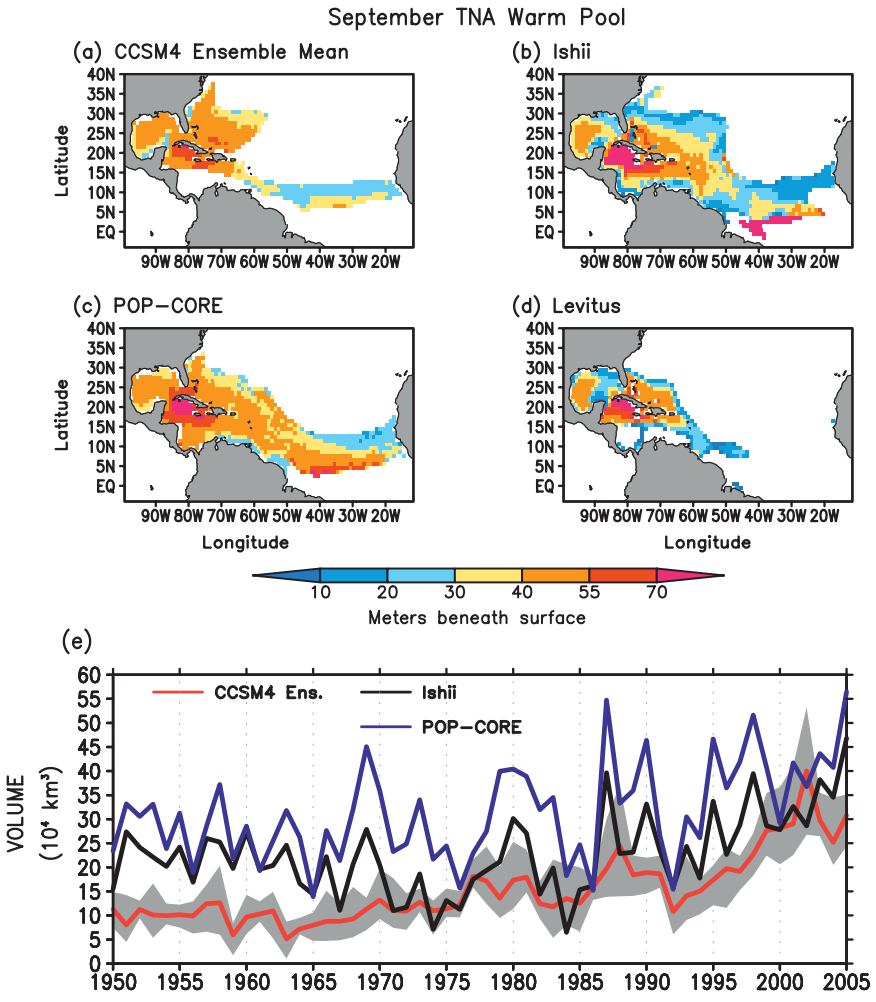

FIG. 6. TNA-WP in September showing the mean depth (m) of the 28.5°C isotherm in September: (a) CCSM4, (b) Ishii, (c) POP-CORE, and (d) Levitus. The CCSM4 ensemble mean is the mean of five different simulations. (e) Time series of the volume (10^4 km^3) encompassed by the 28.5°C isotherm in September north of 5°N. The black line is the I2003 observational products. The blue line is the ocean POP simulation forced by CORE forcing. The red line is the CCSM4 ensemble mean with the ensemble spread in gray. Ensemble spread is the minimum and maximum values of any of the ensemble members.

volumes in the late 1980s and after 1994. Between 1950 and 2005, there are years of decreased observed volume in the mid-1970s (minimum in 1974) and the mid-1980s (minimum in 1984). The POP-CORE hindcast has a similar evolution to I2003 with relative minima in the mid-1970s and in the mid-1980s (even though POP-CORE does not use or assimilate subsurface data). After the 1970s the CCSM4 ensemble spread encompasses the observational estimate or the POP-CORE hindcast. Before the 1970s the CCSM4 warm pool was smaller than the observational estimate and the POP-CORE simulation.

The April time series of TSA volume (km^3) encompassed by the 28.5°C isotherm (i.e., the TSA-WP) are shown in Fig. 7e. The volume was calculated from the 5°N latitude to the south and across the basin. The TSA-WP volume has periods of relative minima in the early 1950s and the late 1970s. Like its northern counterpart, the TSA in the POP-CORE hindcast has a similar evolution to I2003, even though subsurface temperatures are not assimilated in POP-CORE. However, because of the warm bias, the CCSM4 ensemble simulations have a TSA-WP much larger than observations and their spread does not encompass the observational estimates.

Even though the time series of the CCSM4 ensemble simulations do not correspond to the time series from observations, we can compare basic statistics such as the

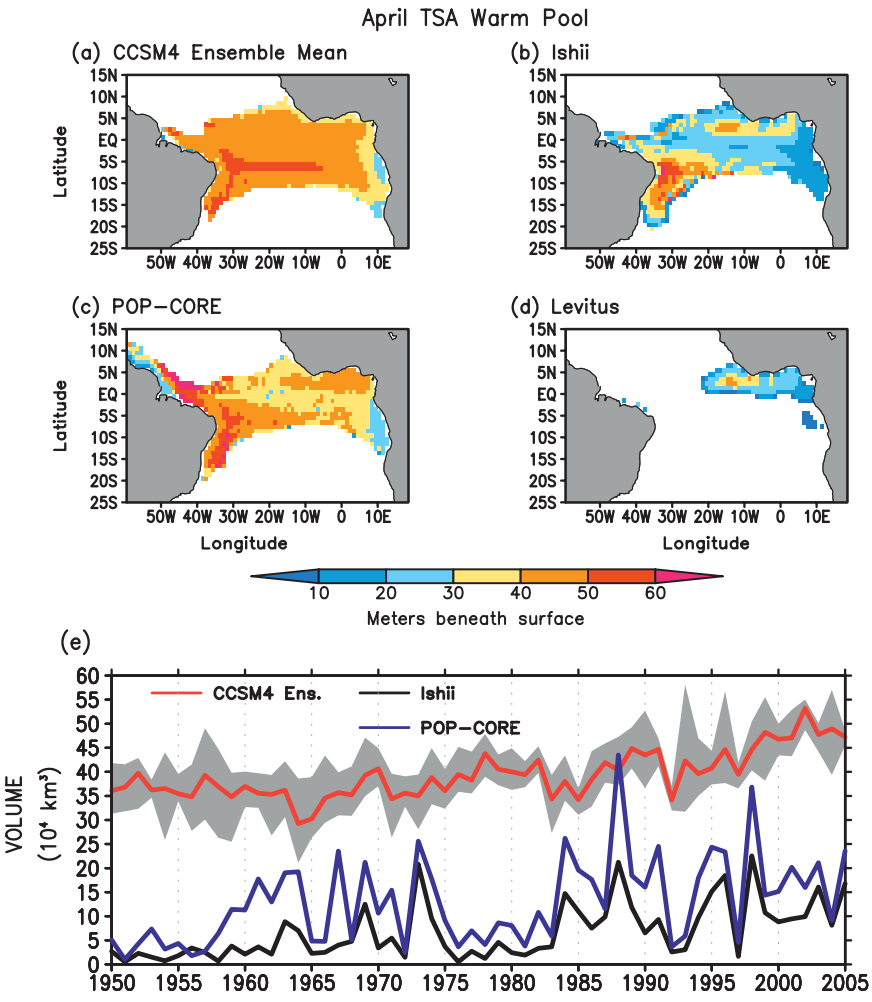

FIG. 7. As in Fig. 6, but for the TSA-WP in April.

trend, the standard deviation, and the autocorrelation of the WP time series. Furthermore, a rank histogram was calculated to determine if the CCSM4 ensemble has undervariability with respect to observations and with respect to the POP-CORE simulation.

The trend of the WP indices of each product (including each ensemble simulation) is shown in Table 1. The trend was calculated from the period 1950–2005. The September TNA-WP in the CCSM4 20C simulations has a greater trend than that of the observational estimate and the POP-CORE simulation. However, the April TSA-WP trends in CCSM4 are about the same as those from observations and the POP-CORE simulation. To analyze other statistics, the long-term mean and the trends in Table 1 were removed from the corresponding WP time series. Then, the standard deviation, autocorrelation, and rank histograms were computed from these detrended time series.

The standard deviations of the WP indices are shown in Table 2. The WP indices from the POP-CORE simulation have the greatest standard deviation of all the products. The TNA-WP in September has a lower standard deviation in CCSM4 than in I2003, but the TSA-WP in April has a greater standard deviation in CCSM4 than in I2003. From a rank histogram analysis

TABLE 1. Linear trend (10^4 km^3 yr^{-1}) of the September TNA-WP and April TSA-WP indices for each CCSM4 ensemble simulation, POP-CORE, and the observational estimates of I2003 (obs). The columns R005–R009 correspond to the ensemble simulations.

Linear trend	R005	R006	R007	R008	R009	POP	Obs
Sep	0.347	0.337	0.355	0.360	0.353	0.283	0.221
Apr	0.184	0.190	0.276	0.196	0.251	0.254	0.207

TABLE 2. As in Table 1, but for std dev.

Std dev	R005	R006	R007	R008	R009	POP	Obs
Sep	6.42	5.00	5.38	5.89	6.31	8.90	7.52
Apr	5.56	4.90	5.35	4.61	5.85	8.14	4.76

(Fig. 8), it can be observed that the CCSM4 TNA-WP has underdispersion with respect to both the I2003 WP and the POP-CORE WP. Yet, the POP-CORE may have excessive interannual variability, as indicated by the low autocorrelation values in Table 3. For the TSA-WP, even though the CCSM4 has undervariability with respect to the POP-CORE, the variability with respect to I2003 is unclear (Fig. 8).

b. *Modes of SST variability*

The dominant rEOFs of SSTs from observations, the CCSM4 ensemble mean, and the POP-CORE experiment are shown in Fig. 9, while the spectra of the associated rotated PCs (rPCs) are shown in Fig. ES-1 in the supplementary material to this paper (http://dx.doi.org/10.1175/JCLI-D-11-00294.s1.) The associated levels of variance accounted for by each of these modes (both in relative and absolute sense) are tabulated in Table 4. The dominant modes in the observations are the so-called patterns of the STA, NTA, and SSA modes (e.g., Huang et al. 2004; Bates 2008, 2010). These modes are represented by the dominant rEOFs of the CCSM4 ensemble members and the POP-CORE experiment, although they account for different levels of variance (Table 4). Note that the rEOFs are not very well separated in terms of explained variance, so the relative order of the modes is not of critical importance.

The NTA and SSA modes are well represented in CCSM4 (Fig. 9, bottom panels) with centers of action located off West Africa and in the central South Atlantic, respectively, as in the observations. The domain-averaged variance of the NTA is underestimated by the ensemble members (0.014 vs 0.022°C^2), making it the weakest mode in all but one of the ensemble members (R008). Nonetheless, the variance accounted for by the SSA mode is well represented (0.019 vs 0.018°C^2). The spectral content of the rPCs of the NTA and SSA modes is consistent with a first-order autoregression (AR1) process, as no significant spectral peaks are present in the ensemble mean nor in the observations (Fig. ES-1). Only the NTA mode in the POP-CORE run displays some enhanced energy at the annual frequency. Lagged correlations between the rPCs and the wind stress (Fig. 10) show that both the NTA and SSA modes (bottom panels) are associated with a weakening of the trade winds, in

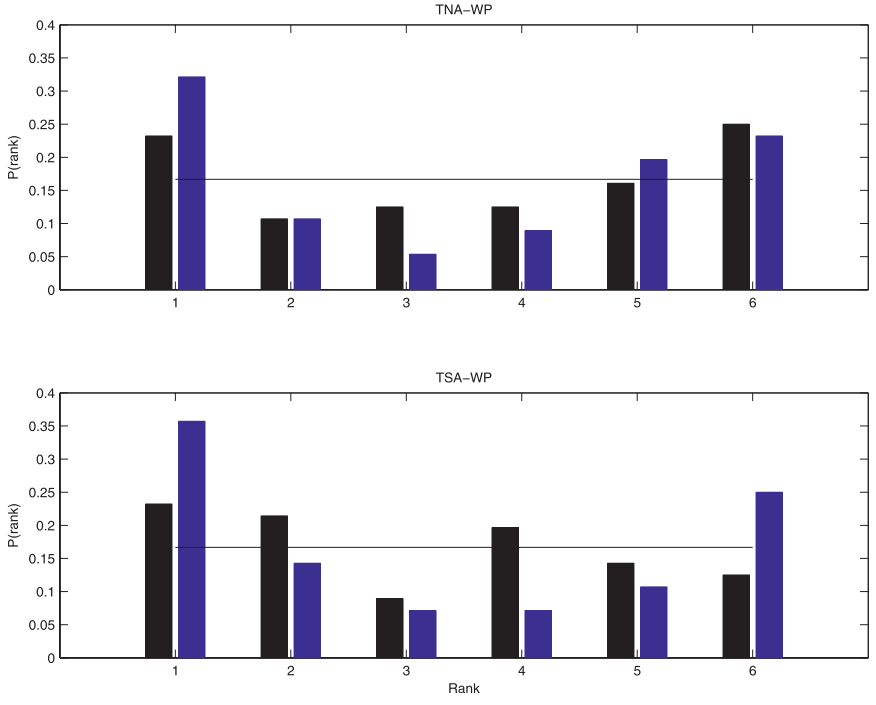

FIG. 8. Rank histograms of the CCSM4 ensemble members against the POP ocean simulation forced by CORE (blue) and against the I2003 observational estimates (black), where (top) corresponds to the index of the TNA-WP in September and (bottom) corresponds to the index of the TSA-WP in April. Black line represents a uniform distribution.

TABLE 3. As in Table 1, but for Spearman (R_a S) and Pearson (R_a P) autocorrelations.

	Autocorrelation	R005	R006	R007	R008	R009	POP	Obs
Sep	R_a S	0.38	0.30	0.31	0.43	0.56	0.17	0.34
	R_a P	0.46	0.35	0.34	0.39	0.49	0.14	0.33
Apr	R_a S	0.18	0.32	0.12	0.18	0.20	0.02	0.13
	R_a P	0.22	0.39	0.10	0.03	0.24	−0.05	0.02

agreement with observations (e.g., Barreiro et al. 2004; Bates 2008). The correlation peaks when wind stress leads by one month. The NTA lead–lag correlations are consistent with the so-called WES feedback that has been proposed as the dominant mechanism for these modes (Chang et al. 1997; Sterl and Hazeleger 2003); a negative wind stress perturbation reduces evaporation and evaporative cooling, inducing a positive SST anomaly that amplifies the wind stress anomaly (Moura and Shukla 1981). The NTA mode is also associated with a

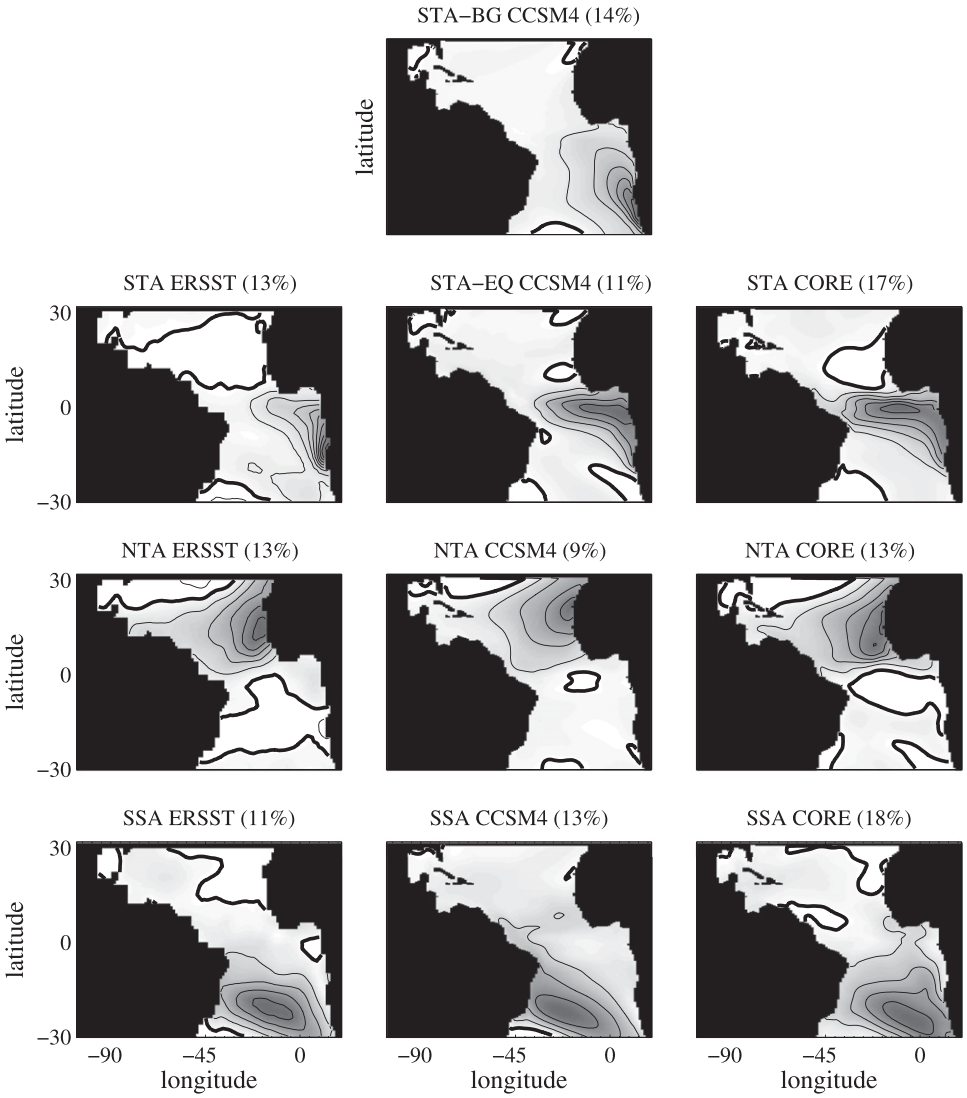

FIG. 9. Dominant rEOFs of SST for the (left) ERSSTv3b dataset, (middle) mean of the five 20C ensemble members of the CCSM4, and (right) CORE-forced ocean–ice simulation. The rEOFs are based on a varimax rotation as explained in the text. NTA and SSA modes are found in all datasets. In CCSM4, the STA variability is represented by the STA-EQ and STA-BG modes. The rEOFs carry the standard deviation. Negative, zero, and positive contours are thin dashed, thick solid, and thin solid, respectively, with a contour interval of 0.1°C.

TABLE 4. Leading rEOFs of SST for the ERSSTv3b dataset, the five 20C ensemble members of CCSM4 (R005–R009), the ensemble mean (Ens), and the CORE-forced ocean–ice simulation. The rEOFs are based on a varimax rotation as explained in text. The second row of the table is the averaged variance ($°C^2$) of the full SST fields. For each mode there are three rows of cells: the first row indicates in bold the relative ordering of the modes, while the second and third rows of cells indicate relative (%) and absolute (domain averaged, $°C^2$) levels of variance accounted for by the modes, respectively. In the CCSM4 ensemble members, the STA variability is represented by the STA-EQ and STA-BG modes.

	ERSST	R005	R006	R007	R008	R009	Ens	CORE
	0.1723	0.1514	0.1486	0.1567	0.1540	0.1478	0.1517	0.1651
STA-BG	—	**1**	**1**	**3**	**1**	**1**	**1**	—
	—	13.6	17.8	11.7	13.7	15.5	14.5	—
	—	0.0206	0.0264	0.0184	0.0211	0.0228	0.0219	—
STA-EQ	**1**	**3**	**2**	**2**	**4**	**3**	**3**	**2**
	12.9	10.6	11.6	13.6	9.5	10.7	11.2	16.8
	0.0223	0.0161	0.0173	0.0213	0.0146	0.0159	0.0170	0.0277
NTA	**2**	**4**	**4**	**4**	**3**	**4**	**4**	**3**
	12.6	9.7	6.9	8.2	10.1	9.5	8.9	13.0
	0.0217	0.0147	0.0103	0.0128	0.0155	0.0141	0.0135	0.0215
SSA	**3**	**2**	**3**	**1**	**2**	**2**	**2**	**1**
	10.7	13.4	11.4	14.3	12.0	11.5	12.5	17.9
	0.0184	0.0203	0.0170	0.0224	0.0185	0.0170	0.0190	0.0296

strengthening of the southeasterly trade winds in the tropical South Atlantic. No such interhemispheric relationship is seen in the SSA mode. Instead, the SSA mode appears to be related to in-phase variability in the tropical South Pacific (Fig. 11).

The largest variability in the ERSST observational STA mode (a standard deviation of close to 1°C) is found off Angola (Fig. 9). The signal attenuates northward and achieves amplitudes below 0.3°C along the equator. In the POP-CORE run, the emphasis of the STA mode is on the equatorial region, lacking energetic SST variability in the Benguela upwelling region. The POP-CORE equatorial emphasis is probably due to an underestimation of wind stress variability resulting from the CORE forcing (not shown; Grodsky et al. 2012). Yet, the CCSM4 model has two separate modes in the tropical South Atlantic. Variability in equatorial SSTs (>0.4°C) in the CCSM4 ensemble runs is well captured by a mode indicated here as STA equator (STA-EQ). The CCSM4 STA-EQ spatial pattern is very similar to the POP-CORE STA spatial pattern. In contrast, the dominant rEOF in all but one (R007) of the ensemble members [here called the STA Benguela (STA-BG) mode] is characterized by strong (>0.6°C) SST variability in the southern segment of the Benguela upwelling zone, off the coast of Namibia. The variability extends northward, but it does not have an equatorial tongue.

Figure 10 (top left) shows that a warm phase of the STA-BG mode is related to a northerly wind stress anomaly that peaks one month in advance, in agreement with the model study of Richter et al. (2010). The spectrum of the corresponding rPC cannot be distinguished from a red-noise process (Fig. ES-1). In the STA-BG mode, the area of highest SST variability also corresponds to the region of maximum mean meridional wind stress and a weak wind stress bias (from December to May) in the model, compared to observations (Fig. 4). From the global perspective (Fig. 11), the STA-BG mode seems to be related to the tropical southeastern Pacific climate.

The STA-EQ mode is highly correlated to wind stress fluctuations in the central equatorial Atlantic that peak about one month earlier (Fig. 10). Also, the wind stress in the central tropical South Atlantic responds to the SST anomaly with a 1-month lag. The spectrum of the ensemble-mean rPCs displays some enhanced energy at a period of about nine months, a feature that does not seem to be present in the rPC of the observational STA mode (Fig. ES1). The CCSM4 STA-EQ mode is collocated with a decrease in SLP anomalies. The SLP anomalies in the tropical Atlantic are anticorrelated with SLP anomalies in the tropical Pacific (Fig. 11). Also, the anticorrelation with the Niño-3 index peaks 9 months after the peak of the STA-EQ mode.

c. *Heat budget of the Benguela region*

For the purposes of this section, the model Benguela index is defined based on the variability of the heat content rate of change (HCR). In the east, where the thermocline is shallower, the regions of high HCR variability are roughly collocated with regions of high SST variability. This is in contrast to the western equatorial Atlantic, where SST variability is relatively weak regardless of rather strong HCR variability. The model Benguela region extends from 20°S to the northern edge of the time-mean SST front at 13°S (where the standard deviation of HCR is ≥250 W m^{-2}) and from 9°E to the coast of southwestern Africa (Fig. 12). Although the observed SST front is mostly confined to the meridional

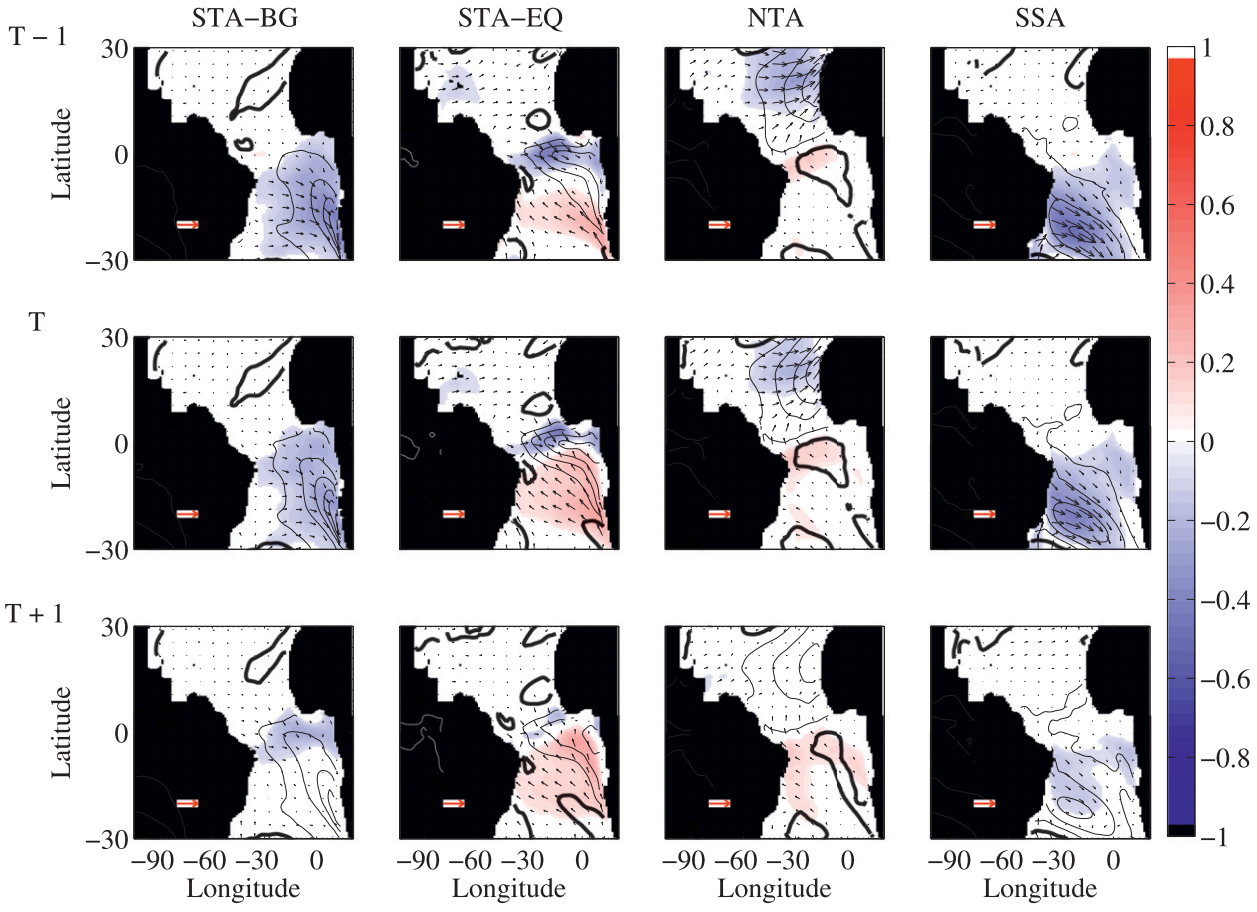

FIG. 10. Statistical relationship between wind stress, SST, and the rPCs of (left to right) the four dominant SST modes (STA-BG, STA-EQ, NTA, and SSA) in the R005 of CCSM4 at lags of (top to bottom) −1, 0, and 1 months. Negative lags indicate the wind stress and SST are leading. Correlations and regressions cover the 1948–2005 period. Shadings correspond to the correlation between the rPCs and wind stress magnitude (only values significant at the 95% level are shown). Arrows correspond to the linear regression of the rPCs on the wind stress components (red legend arrows are 0.0089, 0.0069, 0.0084, and 0.0087 N m^{-2} for the STA-BG, STA-EQ, NTA, and SSA columns, respectively). Contours correspond to the linear regression of the rPCs on the SST (contour interval is 0.1; negative, zero, and positive contours are indicated with gray, thick black, and black, respectively). The rPCs are renormalized to have a standard deviation of 1, so the regressions correspond to unit amplitude of the rPCs.

extent of the Benguela region, the model SST front is stretched farther south (Fig. 12). As a result, the region of high SST variability is also stretched southward. The model Benguela region, as defined above, covers only the northern part of the high model SST variability zone, but it is influenced by both the STA-BG and STA-EQ modes (Fig. 9). This selected northern part is close to the observed region of high SST variability in the Angola–Benguela Front (see, e.g., Florenchie et al. 2003).

In the CCSM4, anomalous SST events in the Benguela region last for approximately four months (Fig. 13). Heat balance analysis based on Eq. (1) suggests that anomalous HCR varies in phase with instantaneous anomalous heat advection and surface flux. In general this is confirmed by correlation analysis of the region-averaged time series, which identifies ocean heat advection as the dominant contribution to the heat budget in the Benguela region. The largest influence is provided by vertical heat advection (upwelling). The magnitude of its correlation with anomalous HCR at zero lag exceeds 0.7; that is, vertical advection accounts for 51% of the anomalous HCR variance. The second strongest contribution is from anomalous meridional heat advection (correlation of 0.5), which accounts for about 26% of the anomalous HCR variance. Anomalous meridional heat advection is dominated by an anomalous meridional current acting on the mean meridional gradient of temperature (as explained by Colberg and Reason 2007a). The impact of zonal advection is weak in CCSM4 due to the predominantly zonal orientation of the isotherms in the Angola–Benguela Front. Local surface flux accounts for only 12% of the anomalous HCR variance. Surface flux

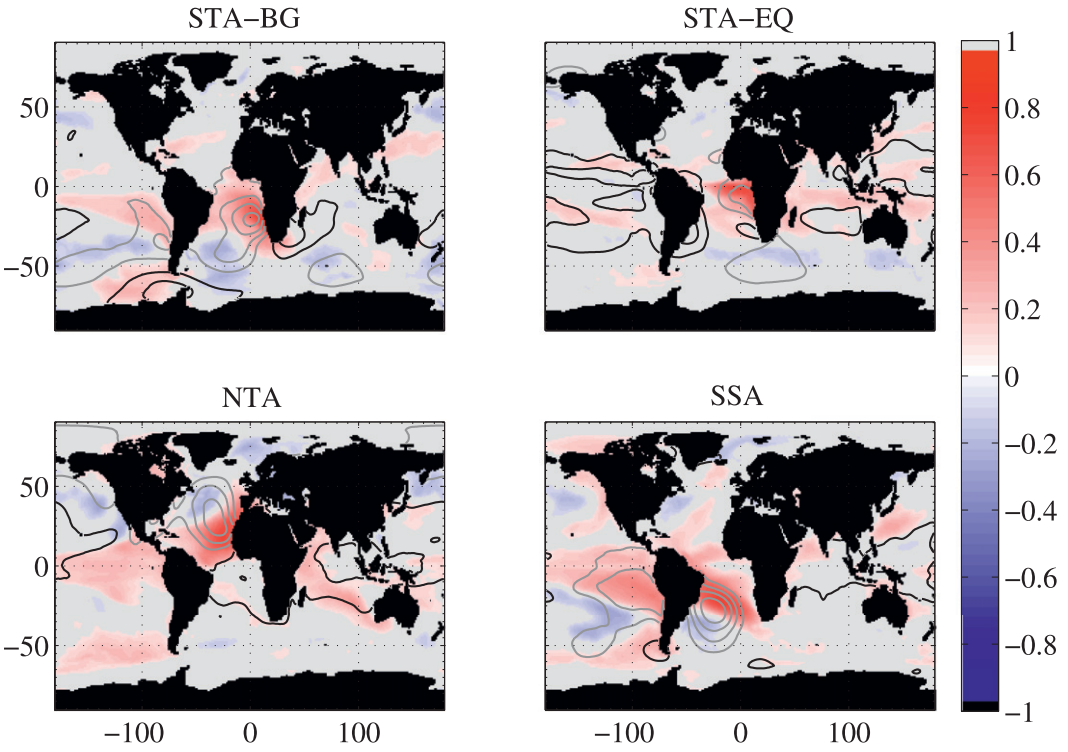

FIG. 11. Lagged correlations between each of the rPCs and SST (shading) or SLP (contours) from the ensemble run R005. Rotated PCs lag by 1 month. The top of each panel indicates the corresponding mode, as explained in the text. Shadings are correlations with SST (gray areas are not significant at the 95% level). Contours are correlations with SLP: black contours are positive and gray contours are negative, with a contour interval of 0.1 starting at ±0.1 (the 0 contour is not plotted).

also provides a weak negative feedback on anomalous SSTs in 2 months after the peak of HCR via latent heat flux.

To explore the possible atmospheric forcing of anomalous heat advection in the Benguela region, the area-averaged time series of anomalous vertical and meridional advection have been lag correlated with wind stress anomalies elsewhere (Fig. 14). This analysis illustrates that anomalously warm vertical advection in the Benguela region (reduced upwelling) occurs in phase with the weakening of southeasterly trade winds. The maximum correlation is at zero lag, suggesting that the impact of local upwelling dominates. This is evident in an anomalous cyclonic wind pattern driven by an anomalously weak South Atlantic subtropical high. The anomalous wind pattern includes a northerly (downwelling) component along the coast. Although the upwelling is attenuated along a major portion of the South African coast, its impact on SST is stronger in the Benguela region, where the thermocline shoals. An interesting (but not yet well understood) feature of the air pressure pattern is the area of anomalously high pressure over South Africa. A zonal gradient between the high over land and the low over the ocean further accelerates anomalous downwelling winds along the coast. An increase in air pressure over the land during warm Benguela events may be linked to cooling of the land due to above-average rainfall along the coasts of Angola

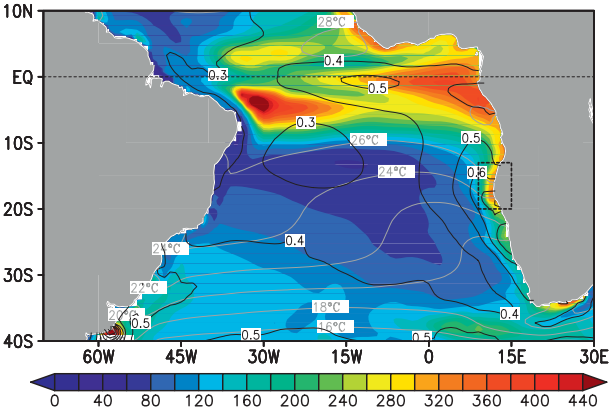

FIG. 12. Standard deviation (std dev) of anomalous HCR in the upper 80 m (shading, W m^{-2}), std dev of anomalous SST (black contours), and time-mean SST (gray contours). Box is the model Benguela region. All data are from the 1° 1850 control run of CCSM4.

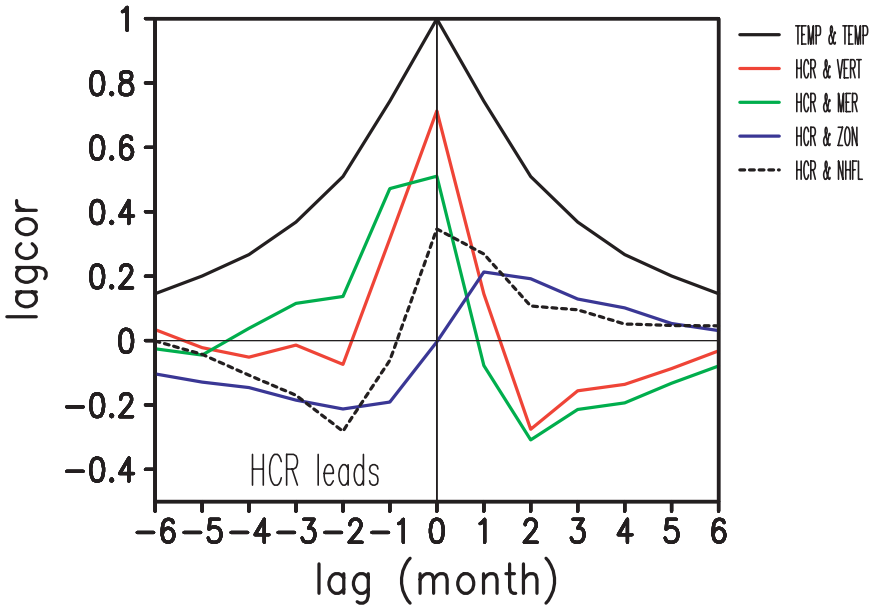

FIG. 13. Lagged autocorrelation of anomalous SST and lagged correlation of anomalous HCR with anomalous vertical (VERT), meridional (MER), zonal (ZON) heat advection, and anomalous net surface heat flux (NHF). All variables are spatially averaged over the Benguela region box and vertically integrated in the upper 80 m.

and Namibia, as observed by Rouault et al. (2003). But in CCSM4 the Benguela SST does not correlate significantly with either land temperature or rainfall.

The wind pattern corresponding to anomalous meridional advection (Fig. 14b) is different from that for anomalous vertical advection (Fig. 14a) in many aspects. For warm Benguela events, the area of weaker southeasterly trades does not cover the Benguela region itself. But, there is significant correlation with the zonal equatorial winds that lead the meridional advection by about a month. This suggests that nonlocal processes translating wind impacts from the equatorial region (such as equatorial and coastal Kelvin waves) are responsible for anomalous meridional heat advection in the Benguela region.

5. Summary and discussion

In this study we assess the CCSM4 with respect to some of the main aspects of the tropical Atlantic mean climate and its variability. We have performed a suite of analyses to address differences and improvements achieved by the CCSM4 in the tropical Atlantic Ocean as compared to observations, an ocean-only POP simulation forced with the CORE dataset (referred to here as the POP-CORE hindcast), and in some occasions CCSM3. Various analyses are presented and discussed covering the main differences in the surface fields, the structure, and interannual variability of the tropical Atlantic warm pools (and therefore of subsurface temperature), and the interannual variability of sea surface temperatures. The variability of the heat budget in the Benguela region was analyzed from a control CCSM4 simulation. The analyses and results presented and discussed will be useful for further evaluations of CCSM4 simulations of the tropical Atlantic climate and for predictive studies of this region. In the following we present a summary of the results.

Both improvements and degradations in the simulated SST occur in the transition from CCSM3 to CCSM4. Some of these differences are related to the changes in the wind stress biases. In CCSM4 there has been a large reduction in the cold biases centered at 20°N as well as in the Caribbean Sea and Gulf of Mexico. This reduction of the cold bias in CCSM4 represents a significant improvement in the simulation of the tropical North Atlantic warm pool (TNA-WP), given that in CCSM3 the TNA-WP was nonexistent (Misra et al. 2009). The CCSM3 warm bias in the southeastern tropical Atlantic upwelling regions was attributed by Chang et al. (2007) to a weak bias in the equatorial easterlies. However, even though the magnitude of equatorial easterlies has improved in CCSM4 (over CCSM3), the warm bias in the southeastern tropical Atlantic is worse in CCSM4 than in CCSM3. Both the reduction of the TNA cold bias and the worsening of the TSA warm

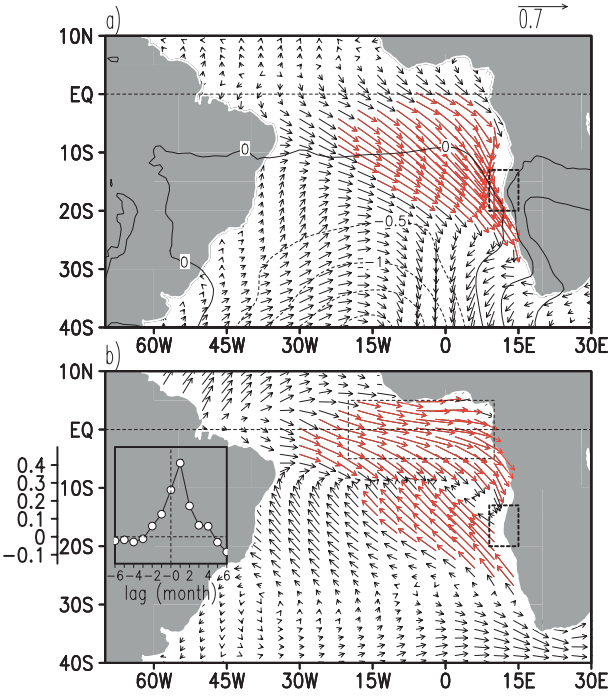

FIG. 14. (a) Correlation of anomalous vertical heat advection in the Benguela region with wind stress elsewhere at 0 lag. Arrows show correlation with wind stress components. Correlations significant at the 95% confidence level are shown in red. Temporal regression of anomalous vertical heat advection on anomalous mean SLP elsewhere at 0 lag is overlain as contours [mbar (100 W m^2)$^{-1}$]. (b) Correlation of anomalous meridional heat advection in the Benguela region with wind stress leading by 1 month. Inlay shows the lagged correlation averaged over the equatorial box. Wind stress leads for positive lags.

bias may be related to the wind stress. They could also be partly due to the overall warming in CCSM4 compared to CCSM3.

The warm pool is analyzed by its vertical structure throughout the year in both the tropical North Atlantic (TNA), including the Intra-Americas Sea (IAS), and the tropical South Atlantic (TSA). The volume of the WP in the tropical South Atlantic (TSA-WP) peaks in April and in the tropical North Atlantic (TNA-WP) it peaks in September. The timing of the seasonal cycle of the WPs in CCSM4 lags that of the observations by about 2 months in either basin. The vertical structure indicates that the TSA-WP pool is deeper in the CCSM4 than in observations. This deeper TSA-WP is related to the CCSM4 warm bias in the TSA region, a common challenge of many coupled models. Regardless of the warm bias, the ensemble spread of the TSA-WP seems to correctly represent the uncertainty or spread of the ensemble.

In the Intra-Americas Sea, the CCSM4 warm pool is smaller than in observations, as a result of the CCSM4 cold bias (and a stronger low-level jet) in the southern Caribbean Sea and to the northeast of the Caribbean Sea. The CCSM smaller warm pool limits the simulation of tropical cyclones by regional models with boundary conditions obtained from CCSM. In particular, Holland et al. (2010) found that given a colder TNA, the CCSM develops a wind vertical shear that is much stronger than observations and therefore inhibits the formation of tropical cyclones. In addition to the CCSM4 simulating a TNA-WP smaller than POP-CORE, the ensemble spread of the TNA-WP is underdispersed compared to the observations. Yet, the trend in the TNA-WP is greater in CCSM4 than in observations, mostly because of a near-monotonic increase in warm pool volume in CCSM4 as opposed to the observational estimates that show large warm pools in the 1950s and 1960s.

To assess the CCSM4 variability of tropical Atlantic SSTs, rotated empirical orthogonal functions (rEOFs) were applied to SST fields of the various CCSM4 ensemble simulations, the POP-CORE simulation, and an observational dataset for the period 1948–2005. The spatial patterns of the main modes of variability in the model are similar to those from the observations. The lead–lag relationship of the rotated principal components (PCs) with wind stress and SST anomalies indicate that the mechanisms of the NTA and SSA modes are consistent with the findings of previous studies. However, in the tropical South Atlantic the coupled model separates the SST variability as two different modes of variability: one centered in the Benguela region (STA-BG) and another one centered along the equator (STA-EQ).

A breakup of the TSA variability in a pattern containing equatorial SST variability and another one capturing variability off Angola seems to be characteristic of at least one other coupled model. Based on analysis of the Center for Ocean–Land–Atmosphere Studies (COLA) AGCM coupled to the Poseidon ocean model, Huang et al. (2004) ascribe this disconnection between equatorial and off-equatorial STA variability to 1) an artificial warm pool related to the intertropical convergence zone (ITCZ) having two preferred locations and 2) two different time scales of SST variability. As a parallel, during March–May, when observations indicate the Benguela variability to be most active (Florenchie et al. 2004), the seasonal wind stress bias in CCSM4 is a reduction, in magnitude and variability, of these southerly coastal winds.

The STA-EQ mode in CCSM4 is characterized by tropical Atlantic SLP variability anticorrelated with tropical Pacific SLP variability and manifested as an interbasin gradient of SLP anomalies (and to a lesser degree an interbasin SST gradient, although not statistically significant). Such an interbasin gradient of SLP

anomalies has been observed (Hastenrath 1990; Giannini et al. 2000; Wang 2006; Muñoz et al. 2008; García-Serrano et al. 2008; Polo et al. 2008) and is increasingly recognized as an intrinsic mode of tropical Atlantic variability that feeds back onto tropical Pacific climate anomalies (García-Serrano et al. 2008; Losada et al. 2010; Ding et al. 2012).

Analysis of the model heat budget in the Benguela region suggests that anomalous vertical advection accounts for about 50% of the anomalous heat content rate (HCR) variance, while the contribution by anomalous meridional heat advection is half as strong. Local surface flux accounts for only 12% of the anomalous HCR variance. The impact of zonal advection is weak. Anomalously warm vertical advection in the Benguela region (reduced upwelling) occurs in phase with the weakening of southeasterly trade winds. Correlation is at a maximum at zero lag, suggesting that the impact of local upwelling dominates. In contrast to vertical heat advection, the anomalous meridional heat advection is forced by zonal equatorial winds, which lead it by about a month. This suggests that nonlocal processes translating wind impacts from the equatorial region (such as equatorial and coastal Kelvin waves) are responsible for anomalous meridional heat advection in the Benguela region. In distinction from observations of Florenchie et al. (2003), this wave-based teleconnection is not the dominant mechanism of heat content variability in the Benguela region in CCSM4.

Acknowledgments. We thank all the scientists and software engineers who contributed to the development of the CCSM4. Computational resources were provided by the Climate Simulation Laboratory at NCAR's Computational and Information Systems Laboratory (CISL), sponsored by the National Science Foundation and other agencies. The CCSM is also sponsored by the Department of Energy. We also wish to thank the staff of the Earth System Grid (including Gary Strand from NCAR) and Mathew Maltrud (from LANL) for the support and contribution in downloading and facilitating data used in this study. The Earth System Grid is funded by the U.S. Department of Energy (DOE). Ernesto Muñoz and Wilber Weijer were supported by the Regional and Global Climate Modeling program of the DOE's Office of Science, and by NSF-OCE Award 0928473. Ilana Wainer was supported by CNPq-MCT/INCT and FAPESP. Semyon Grodsky was supported by NOAA's Climate Variability and Predictability (CVP) program. We thank Marlos Goes, Alicia Karspeck, and the anonymous reviewers for their helpful comments.

REFERENCES

Barreiro, M., A. Giannini, P. Chang, and R. Saravanan, 2004: On the role of the South Atlantic atmospheric circulation in tropical Atlantic variability. *Earth's Climate: The Ocean-Atmosphere Interaction, Geophys. Monogr.,* Vol. 147, Amer. Geophys. Union, 143–156.

Bates, S. C., 2008: Coupled ocean–atmosphere interaction and variability in the tropical Atlantic Ocean with and without an annual cycle. *J. Climate,* **21,** 5501–5523.

——, 2010: Seasonal influences on coupled ocean–atmosphere variability in the tropical Atlantic Ocean. *J. Climate,* **23,** 582–604.

——, B. Fox-Kemper, S. R. Jayne, W. G. Large, S. Stevenson, and S. G. Yeager, 2012: Mean biases, variability, and trends in air–sea fluxes and sea surface temperature in the CCSM4. *J. Climate,* in press.

Carton, J. A., and B. Huang, 1994: Warm events in the tropical Atlantic. *J. Phys. Oceanogr.,* **24,** 888–903.

——, X. Cao, B. S. Giese, and A. M. da Silva, 1996: Decadal and interannual SST variability in the tropical Atlantic Ocean. *J. Phys. Oceanogr.,* **26,** 1165–1175.

Chang, C.-Y., J. A. Carton, S. A. Grodsky, and S. Nigam, 2007: Seasonal climate of the tropical Atlantic sector in the NCAR Community Climate System Model 3: Error structure and probable causes of errors. *J. Climate,* **20,** 1053–1070.

Chang, P., L. Ji, and H. Li, 1997: A decadal climate variation in the tropical Atlantic Ocean from thermodynamic air-sea interactions. *Nature,* **385,** 516–518.

Colberg, F., and C. J. C. Reason, 2007a: A model investigation of internal variability in the Angola Benguela Frontal Zone. *J. Geophys. Res.,* **112,** C07008, doi:10.1029/2006JC003920.

——, and ——, 2007b: Ocean model diagnosis of low-frequency climate variability in the South Atlantic region. *J. Climate,* **20,** 1016–1034.

Czaja, A., P. van der Vaart, and J. Marshall, 2002: A diagnostic study of the role of remote forcing in tropical Atlantic variability. *J. Climate,* **15,** 3280–3290.

Dai, A., K. Trenberth, and T. Qian, 2004: A global dataset of Palmer drought severity index for 1870–2002: Relationship with soil moisture and effects of surface warming. *J. Hydrometeor.,* **5,** 1117–1130.

Danabasoglu, G., S. C. Bates, B. P. Briegleb, S. R. Jayne, M. Jochum, W. G. Large, S. Peacock, and S. G. Yeager, 2012a: The CCSM4 ocean component. *J. Climate,* **25,** 1361–1389.

——, S. G. Yeager, Y.-O. Kwon, J. J. Tribbia, A. S. Phillips, and J. W. Hurrell, 2012b: Variability of the Atlantic meridional overturning circulation in CCSM4. *J. Climate,* in press.

Davey, M. K., and Coauthors, 2002: STOIC: A study of coupled model climatology and variability in tropical ocean regions. *Climate Dyn.,* **18,** 403–420.

Deser, C., A. Capotondi, R. Saravanan, and A. S. Phillips, 2006: Tropical Pacific and Atlantic climate variability in CCSM3. *J. Climate,* **19,** 2451–2481.

Ding, H., N. S. Keenlyside, and M. Latif, 2012: Impact of the equatorial Atlantic on the El Niño Southern Oscillation. *Climate Dyn.,* **38,** 1965–1972, doi:10.1007/s00382-011-1097-y.

Doi, T., T. Tozuka, and T. Yamagata, 2010: The Atlantic meridional mode and its coupled variability with the Guinea Dome. *J. Climate,* **23,** 455–475.

——, G. A. Vecchi, A. J. Rosati, and T. L. Delworth, 2012: Biases in the Atlantic ITCZ in seasonal–interannual variations for a coarse- and a high-resolution coupled climate model. *J. Climate,* in press.

Dommenget, D., and M. Latif, 2000: Interannual to decadal variability in the tropical Atlantic. *J. Climate,* **13,** 777–792.

——, and ——, 2002: A cautionary note on the interpretation of EOFs. *J. Climate,* **15,** 216–225.

Enfield, D. B., and D. Mayer, 1997: Tropical Atlantic sea surface temperature variability and its relation to El Niño-Southern Oscillation. *J. Geophys. Res.,* **102** (C1), 929–945.

——, and S.-K. Lee, 2005: The heat balance of the Western Hemisphere warm pool. *J. Climate,* **18,** 2662–2681.

——, A. M. Mestas-Nuñez, and P. J. Trimble, 2001: The Atlantic multidecadal oscillation and its relation to rainfall and river flows in the continental U.S. *Geophys. Res. Lett.,* **28,** 2077–2080.

Florenchie, P., J. R. E. Lutjeharms, C. J. C. Reason, S. Masson, and M. Rouault, 2003: The source of Benguela Niños in the South Atlantic Ocean. *Geophys. Res. Lett.,* **30,** 1505, doi:10.1029/2003GL017172.

——, C. J. C. Reason, J. R. E. Lutjeharms, and M. Rouault, 2004: Evolution of interannual warm and cold events in the southeast Atlantic Ocean. *J. Climate,* **17,** 2318–2334.

Foltz, G. R., and M. J. McPhaden, 2010: Interaction between the Atlantic meridional and Niño modes. *Geophys. Res. Lett.,* **37,** L18604, doi:10.1029/2010GL044001.

García-Serrano, J., T. Losada, B. Rodríguez-Fonseca, and I. Polo, 2008: Tropical Atlantic variability modes (1979–2002). Part II: Time-evolving atmospheric circulation related to SST-forced tropical convection. *J. Climate,* **21,** 6476–6497.

Garzoli, S. L., and J. Servain, 2003: CLIVAR workshop on tropical Atlantic variability. *Geophys. Res. Lett.,* **30,** 8001, doi:10.1029/2002GL016823.

Gent, P. R., F. O. Bryan, G. Danabasoglu, K. Lindsay, D. Tsumune, M. W. Hecht, and S. C. Doney, 2006: Ocean chlorofluorocarbon and heat uptake during the twentieth century in the CCSM3. *J. Climate,* **19,** 2366–2381.

——, and Coauthors, 2011: The Community Climate System Model version 4. *J. Climate,* **24,** 4973–4991.

Giannini, A., Y. Kushnir, and M. A. Cane, 2000: Interannual variability of Caribbean rainfall, ENSO, and the Atlantic Ocean. *J. Climate,* **13,** 297–311.

Gray, W. M., 1990: Strong association between West African rainfall and U.S. landfall of intense hurricanes. *Science,* **249,** 1251–1256.

Griffies, S. M., and Coauthors, 2009: Coordinated Ocean-Ice Reference Experiments (COREs). *Ocean Modell.,* **26,** 1–46.

Grodsky, S. A., J. A. Carton, S. Nigam, and Y. M. Okumura, 2012: Tropical Atlantic biases in CCSM4. *J. Climate,* **25,** 3684–3701.

Hamill, T. M., 2001: Interpretation of rank histograms for verifying ensemble forecasts. *Mon. Wea. Rev.,* **129,** 550–560.

Hastenrath, S., 1990: Diagnostics and prediction of anomalous river discharge in northern South America. *J. Climate,* **3,** 1080–1096.

——, and L. Heller, 1977: Dynamics of climatic hazards in Northeast Brazil. *Quart. J. Roy. Meteor. Soc.,* **103,** 77–92.

Hirst, A. C., and S. Hastenrath, 1983: Atmosphere–ocean mechanisms of climate anomalies in the Angola–tropical Atlantic sector. *J. Phys. Oceanogr.,* **13,** 1146–1157.

Holland, G. J., J. M. Done, C. L. Bruyere, C. Cooper, and A. Suzuki-Parker, 2010: Model investigations of the effects of climate variability and change on future Gulf of Mexico tropical cyclone activity. *Proc. Offshore Technology Conf.,* Houston, TX, OTC, 20690-MS, 13 pp.

Holland, M. M., D. A. Bailey, B. P. Briegleb, B. Light, E. Hunke, 2012: Improved sea ice shortwave radiation physics in CCSM4: The impact of melt ponds and aerosols on Arctic sea ice. *J. Climate,* **25,** 1413–1430.

Hu, Z.-Z., and B. Huang, 2007: Physical processes associated with the tropical Atlantic SST gradient during the anomalous evolution in the southeastern ocean. *J. Climate,* **20,** 3366–3378.

——, ——, and K. Pegion, 2008: Leading patterns of the tropical Atlantic variability in a coupled general circulation model. *Climate Dyn.,* **30,** 703–726, doi:10.1007/s00382-007-0318-x.

Huang, B., and J. Shukla, 2005: Ocean–atmosphere interactions in the tropical and subtropical Atlantic Ocean. *J. Climate,* **18,** 1652–1672.

——, P. S. Schopf, and J. Shukla, 2004: Intrinsic ocean–atmosphere variability of the tropical Atlantic Ocean. *J. Climate,* **17,** 2058–2077.

Hurrell, J. W., and Coauthors, 2006: Atlantic climate variability and predictability: A CLIVAR perspective. *J. Climate,* **19,** 5100–5121.

——, J. J. Hack, D. Shea, J. M. Caron, and J. Rosinski, 2008: A new sea surface temperature and sea ice boundary dataset for the Community Atmosphere Model. *J. Climate,* **21,** 5145–5153.

Ishii, M., M. Kimoto, and M. Kachi, 2003: Historical ocean subsurface temperature analysis with error estimates. *Mon. Wea. Rev.,* **131,** 51–73.

Keenlyside, N. S., and M. Latif, 2007: Understanding equatorial Atlantic interannual variability. *J. Climate,* **20,** 131–142.

Kucharski, F., A. Bracco, J. H. Yoo, and F. Molteni, 2007: Low-frequency variability of the Indian monsoon–ENSO relationship and the tropical Atlantic: The ''weakening'' of the 1980s and 1990s. *J. Climate,* **20,** 4255–4266.

——, ——, ——, and ——, 2008: Atlantic forced component of the Indian monsoon interannual variability. *Geophys. Res. Lett.,* **35,** L04706, doi:10.1029/2007GL033037.

——, ——, ——, A. Tompkins, L. Feudale, P. Ruti, and A. Dell'Aquila, 2009: A Gill-Matsuno-type mechanism explains the tropical Atlantic influence on African and Indian monsoon rainfall. *Quart. J. Roy. Meteor. Soc.,* **135,** 569–579.

Landsea, C. W., R. A. Pielke Jr., A. M. Mestas-Nuñez, and J. A. Knaff, 1999: Atlantic basin hurricanes: Indices of climatic changes. *Climatic Change,* **42,** 89–129.

Large, W. G., and G. Danabasoglu, 2006: Attribution and impacts of upper-ocean biases in CCSM3. *J. Climate,* **19,** 2325–2346.

——, and S. Yeager, 2009: The global climatology of an interannually varying air–sea flux data set. *Climate Dyn.,* **33,** 341–364.

Lee, S.-K., D. B. Enfield, and C. Wang, 2007: What drives the seasonal onset and decay of the Western Hemisphere warm pool? *J. Climate,* **20,** 2133–2146.

Levitus, S., and Coauthors, 1998: *Introduction.* Vol. 1, *World Ocean Atlas 1998,* NOAA Atlas NESDIS 18, 346 pp.

Locarnini, R. A., A. V. Mishonov, J. I. Antonov, T. P. Boyer, H. E. Garcia, O. K. Baranova, M. M. Zweng, and D. R. Johnson, 2010: *Temperature.* Vol. 1, *World Ocean Atlas 2009,* NOAA Atlas NESDIS 68, 184 pp. [Available online at ftp://ftp.nodc.noaa.gov/pub/WOA09/DOC/woa09_vol1_text.pdf.]

Losada, T., B. Rodríguez-Fonseca, I. Polo, S. Janicot, S. Gervois, F. Chauvin, and P. Ruti, 2010: Tropical response to the Atlantic equatorial mode: AGCM multimodel approach. *Climate Dyn.,* **35,** 45–52, doi:10.1007/s00382-009-0624-6.

Lübbecke, J. F., C. W. Böning, N. S. Keenlyside, and S.-P. Xie, 2010: On the connection between Benguela and equatorial Atlantic Niños and the role of the South Atlantic anticyclone. *J. Geophys. Res.,* **115,** C09015, doi:10.1029/2009JC005964.

Ma, C.-C., C. R. Mechoso, A. W. Robertson, and A. Arakawa, 1996: Peruvian stratus clouds and the tropical Pacific circulation: A coupled ocean–atmosphere CGM study. *J. Climate,* **9,** 1635–1645.

Mahajan, S., R. Saravanan, and P. Chang, 2010: Free and forced variability of the tropical Atlantic Ocean: Role of the wind–evaporation–sea surface temperature feedback. *J. Climate,* **23,** 5958–5977.

Medeiros, B., 2011: Comparing the Southern Hemisphere stratocumulus decks in the Community Atmosphere Model. *Variations,* No. 2, U.S. CLIVAR Office, Washington, DC, 5–8.

Misra, V., S. Chan, R. Wu, and E. Chassignet, 2009: Air-sea interaction over the Atlantic warm pool in the NCEP CFS. *Geophys. Res. Lett.,* **36,** L15702, doi:10.1029/2009GL038737.

Moura, A. D., and J. Shukla, 1981: On the dynamics of droughts in Northeast Brazil: Observations, theory and numerical experiments with a general circulation model. *J. Atmos. Sci.,* **38,** 2653–2675.

Muñoz, E., A. J. Busalacchi, S. Nigam, and A. Ruiz-Barradas, 2008: Winter and summer structure of the Caribbean low-level jet. *J. Climate,* **21,** 1260–1276.

——, C. Wang, and D. Enfield, 2010: The Intra-Americas springtime sea surface temperature anomaly dipole as fingerprint of remote influences. *J. Climate,* **23,** 43–56.

——, B. Kirtman, and W. Weijer, 2011: Varied representation of the Atlantic meridional overturning circulation in ocean reanalyses. *Deep-Sea Res. II,* **58,** 1848–1857.

Murtugudde, R. G., J. Ballabrera-Poy, J. Beauchamp, and A. J. Busalacchi, 2002: Relationship between zonal and meridional modes in the tropical Atlantic. *Geophys. Res. Lett.,* **22,** 4463–4466.

Nicholson, S. E., 2010: A low-level jet along the Bengueal coast, an intergral part of the Benguela Current ecosystem. *Climatic Change,* **99,** 613–624.

Nobre, P., and J. Shukla, 1996: Variations of sea surface temperature, wind stress, and rainfall over the tropical Atlantic and South America. *J. Climate,* **9,** 2464–2479.

Philander, S. G. H., D. Gu, D. Halpern, G. Lambert, N.-C. Lau, T. Li, and R. C. Pacanowski, 1996: Why the ITCZ is mostly north of the equator. *J. Climate,* **9,** 2958–2972.

Polo, I., B. Rodriguez-Fonseca, T. Losada, and J. García-Serrano, 2008: Tropical Atlantic variability modes (1979–2002). Part I: Time-evolving SST modes related to West African rainfall. *J. Climate,* **21,** 6457–6475.

Richman, M. B., 1986: Rotation of principal components. *J. Climatology,* **6,** 293–335.

Richter, I., and S.-P. Xie, 2008: On the origin of equatorial Atlantic biases in coupled general circulation models. *Climate Dyn.,* **31,** 587–598.

——, S. K. Behera, Y. Masumoto, B. Taguchi, N. Komori, and T. Yamagata, 2010: On the triggering of Benguela Niños: Remote equatorial versus local influences. *Geophys. Res. Lett.,* **37,** L20604, doi:10.1029/2010GL044461.

——, S.-P. Xie, A. T. Wittenberg, and Y. Masumoto, 2012: Tropical Atlantic biases and their relation to surface wind stress and terrestrial precipitation. *Climate Dyn.,* **38,** 985–1001, doi:10.1007/s00382-011-1038-9.

Robertson, A. W., J. D. Farrara, and C. R. Mechoso, 2003: Simulations of the atmospheric response to South Atlantic sea surface temperature anomalies. *J. Climate,* **16,** 2540–2551.

Rouault, M., P. Florenchie, N. Fauchereau, and C. J. C. Reason, 2003: South East tropical Atlantic warm events and southern African rainfall. *Geophys. Res. Lett.,* **30,** 8009, doi:10.1029/2002GL014840.

——, S. Illig, C. Bartholomae, C. J. C. Reason, and A. Bentamy, 2007: Propagation and origin of warm anomalies in the Angola Benguela upwelling system in 2001. *J. Mar. Syst.,* **68,** 473–488.

——, J. Servain, C. J. C. Reason, B. Bourles, M. J. Rouault, and N. Fauchereau, 2009: Extension of PIRATA in the tropical south-east Atlantic: An initial one-year experiment. *Afr. J. Mar. Sci.,* **31,** 63–71.

Ruiz-Barradas, A., J. A. Carton, and S. Nigam, 2000: Structure of interannual-to-decadal climate variabilty in the tropical Atlantic sector. *J. Climate,* **13,** 3285–3297.

Saravanan, R., and P. Chang, 2000: Interactions between the Pacific ENSO and tropical Atlantic climate variability. *J. Climate,* **13,** 2177–2194.

Schouten, M. W., R. P. Matano, and T. P. Strub, 2005: A description of the seasonal cycle of the equatorial Atlantic from altimeter data. *Deep-Sea Res. I,* **52,** 477–493.

Servain, J., 1991: Simple climatic indices for the tropical Atlantic Ocean and some applications. *J. Geophys. Res.,* **96** (C8), 15 137–15 146.

——, M. Séva, and P. Rual, 1990: Climatology comparison and long-term variations of sea surface temperature over the tropical Atlantic Ocean. *J. Geophys. Res.,* **95** (C6), 9421–9431.

——, A. J. Busalacchi, M. J. McPhaden, A. D. Moura, G. Reverdin, M. Vianna, and S. E. Zebiak, 1998: A Pilot Research Moored Array in the Tropical Atlantic (PIRATA). *Bull. Amer. Meteor. Soc.,* **79,** 2019–2031.

——, G. Clauzet, and I. C. Wainer, 2003: Modes of tropical Atlantic climate variability observed by PIRATA. *Geophys. Res. Lett.,* **30,** 8003,doi:10.1029/2002GL015124.

Shannon, L. V., A. J. Boyd, G. B. Bundrit, and J. Taunton-Clark, 1986: On the existence of an El Niño-type phenomenon in the Benguela system. *J. Mar. Sci.,* **44,** 495–520.

——, J. J. Agenbag, and M. E. L. Buys, 1987: Large- and mesoscale features of the Angola-Benguela Front. *S. Afr. J. Mar. Sci.,* **5,** 11–34.

Small, R. J., S. de Szoeke, and S.-P. Xie, 2007: The Central American midsummer drought: Regional aspects and large-scale forcing. *J. Climate,* **20,** 4853–4873.

Smith, T. M., R. W. Reynolds, T. C. Peterson, and J. Lawrimore, 2008: Improvements to NOAA's historical merged land–ocean surface temperature analysis (1880–2006). *J. Climate,* **21,** 2283–2296.

Sterl, A., and W. Hazeleger, 2003: Coupled variability and air-sea interaction in the South Atlantic Ocean. *Climate Dyn.,* **21,** 559–571, doi:10.1007/s00382-003-0348-y.

Tian, B., G. J. Zhang, and V. Ramanathan, 2001: Heat balance in the Pacific warm pool atmosphere during TOGA COARE and CEPEX. *J. Climate,* **14,** 1881–1893.

Tokinaga, H., and S.-P. Xie, 2011: Weakening of the equatorial Atlantic cold tongue over the past six decades. *Nat. Geosci.,* **4,** 222–226, doi:10.1038/ngeo1078.

Tozuka, T., T. Doi, T. Miyasaka, N. Keenlyside, T. Yamagata, 2011: Key factors in simulating the equatorial Atlantic zonal sea surface temperature gradient in a coupled general circulation model. *J. Geophys. Res.,* **116,** C06010, doi:10.1029/2010JC006717.

Visbeck, M., G. Reverdin, F. Schott, J. Carton, A. Clarke, B. Owens, and D. Stammer, 2001: Atlantic climate variability experiment. *Observing the Oceans in the 21st Century: A Strategy for Global Ocean Observations,* C. J. Koblinsky and N. R. Smith, Eds., Bureau of Meteorology, 445–452.

von Storch, H., 2002: *Statistical Analysis in Climate Research.* Cambridge University Press, 484 pp.

Wahl, S., M. Latif, W. Park, and N. Keenlyside, 2011: On the tropical Atlantic SST warm bias in the Kiel Climate Model. *Climate Dyn.,* **36,** 891–906.

Wang, C., 2006: An overlooked feature of tropical climate: Inter-Pacific-Atlantic variability. *Geophys. Res. Lett.,* **33,** L12702, doi:10.1029/2006GL026324.

——, and D. B. Enfield, 2003: A further study of the tropical Western Hemisphere warm pool. *J. Climate,* **16,** 1476–1493.

——, ——, S.-K. Lee, and C. W. Landsea, 2006: Influences of Atlantic warm pool on Western Hemisphere summer rainfall and Atlantic hurricanes. *J. Climate,* **19,** 3011–3028.

——, S.-K. Lee, and D. Enfield, 2008: Climate response to anomalously large and small Atlantic warm pools during the summer. *J. Climate,* **21,** 2437–2450.

Xie, S.-P., and J. A. Carton, 2004: Tropical Atlantic variability: Patterns, mechanisms, and impacts. *Earth's Climate: The Ocean-Atmosphere Interaction, Geophys. Monogr.,* Vol. 147, Amer. Geophys. Union, 121–142.

Zebiak, S. E., 1993: Air–sea interaction in the equatorial Atlantic region. *J. Climate,* **6,** 1567–1586.

Zuidema, P., P. Chang, C. R. Mechoso, and L. Terray, 2011: Coupled ocean-atmosphere-land processes in the tropical Atlantic. *CLIVAR Exchanges,* No. 1, International CLIVAR Project Office, Southampton, United Kingdom, 12–14.